



**INSTITUTO POTOSINO DE INVESTIGACIÓN  
CIENTÍFICA Y TECNOLÓGICA, A.C.**

**POSGRADO EN CIENCIAS APLICADAS**

**A repetitive-based controller for the compensation of  $6\ell \pm 1$   
harmonic components.**

Tesis que presenta

**Perla Gisel Hernández Briones**

Para obtener el grado de

**Maestro en Ciencias Aplicadas**

En la opción de

**Control y Sistemas Dinámicos**

**Director de la Tesis:**

Dr. Gerardo Escobar Valderrama

San Luis Potosí, S.L.P., Noviembre de 2007



## Créditos Institucionales

Esta tesis fue elaborada en la División de Matemáticas Aplicadas y Sistemas Computacionales del Instituto Potosino de Investigación Científica y Tecnológica, A.C., bajo la dirección del Dr. Gerardo Escobar Valderrama.



INSTITUTO POTOSINO  
DE INVESTIGACIÓN  
CIENTÍFICA Y TECNOLÓGICA, A.C.

IPICYT

## Constancia de aprobación de la tesis

La tesis “A repetitive-based controller for the compensation of  $6l \pm 1$  harmonic components” presentada para obtener el Grado de Maestro en Ciencias Aplicadas en la opción de Control y Sistemas Dinámicos fue elaborada por Perla Gisel Hernández Briones y aprobada el 30 de Noviembre del 2007 por los suscritos, designados por el Colegio de Profesores de la División de Matemáticas Aplicadas del Instituto Potosino de Investigación Científica y Tecnológica, A.C.

Dr. Gerardo Escobar Valderrama  
(Director de la tesis)

Dr. Pánfilo Raymundo Martínez Rodríguez  
(Sinodal)

Dr. Arturo Zavala Río  
(Sinodal)



**IPICYT**

# Instituto Potosino de Investigación Científica y Tecnológica, A.C.

## Acta de Examen de Grado

El Secretario Académico del Instituto Potosino de Investigación Científica y Tecnológica, A.C., certifica que en el Acta 015 del Libro Primero de Actas de Exámenes de Grado del Programa de Maestría en Ciencias Aplicadas en la opción de Control y Sistemas Dinámicos está asentado lo siguiente:

En la ciudad de San Luis Potosí a los 30 días del mes de noviembre del año 2007, se reunió a las 17:00 horas en las instalaciones del Instituto Potosino de Investigación Científica y Tecnológica, A.C., el Jurado integrado por:

<b>Dr. Pánfilo Raymundo Martínez Rodríguez</b>	<b>Presidente</b>	<b>ITESI</b>
<b>Dr. Gerardo Escobar Valderrama</b>	<b>Secretario</b>	<b>IPICYT</b>
<b>Dr. Arturo Zavala Río</b>	<b>Sinodal</b>	<b>IPICYT</b>

a fin de efectuar el examen, que para obtener el Grado de:

**MAESTRA EN CIENCIAS APLICADAS  
EN LA OPCIÓN DE CONTROL Y SISTEMAS DINÁMICOS**

sustentó la C.

**Perla Gisel Hernández Briones**

sobre la Tesis intitulada:

*A repetitive-based controller for the compensation of 6l +/- 1 harmonic components*

que se desarrolló bajo la dirección de


**Dr. Gerardo Escobar Valderrama**

El Jurado, después de deliberar, determinó

**APROBARLA**

Dándose por terminado el acto a las 18:00 horas, procediendo a la firma del Acta los integrantes del Jurado. Dando fé el Secretario Académico del Instituto.

A petición de la interesada y para los fines que a la misma convengan, se extiende el presente documento en la ciudad de San Luis Potosí, S.L.P., México, a los 30 días del mes noviembre de 2007.

  
**L.C.C. Ivonne Lizette Cuevas Velez**  
Jefa del Departamento de Asuntos Escolares

  
**Dr. Marcial Bonilla Marín**  
Secretario Académico



# Agradecimientos

Agradezco a las personas que contribuyeron de una u otra forma a que esta tesis se llevara a cabo.

Perla Gisel Hernández Briones, San Luis Potosí, México. Noviembre del 2007

## LIST OF ACRONYMS

DC or dc	Direct Current
DSP	Digital Signal Processor
LPF	Low Pass Filter
LTI	Linear Time Invariant
PI	Proportional Plus Integral
PWM	Pulse Width Modulation
PR	Positive Real
SPR	Strictly Positive Real
DSP	Digital Signal Processor
BBD	Bucket Brigade Delay



## RESUMEN

En este trabajo de tesis se propone un nuevo esquema de control basado en control repetitivo. La importancia de este controlador radica en su capacidad de compensar distorsión armónica cuyos componentes sean muy específicos, en particular armónicos  $6\ell \pm 1$ , ( $\ell = 0, 1, 2, \dots, \infty$ ) múltiplos de la frecuencia fundamental  $\omega_0$ , esto es, los armónicos 1, 5, 7, 11, etc.

Una contribución de esta tesis es la introducción de amortiguamiento al esquema repetitivo propuesto, con lo cual, éste pasa de ser un banco de filtros resonantes a ser un banco de filtros pasabanda. En otras palabras, el controlador pasa de tener ganancia infinita en los múltiplos  $(6\ell \pm 1)\omega_0$  a tener ganancia finita, evitando de esta manera posibles problemas de inestabilidad. Sin embargo, al introducir este amortiguamiento al controlador, se introduce también un ligero desfase en los picos de resonancia. Para eliminar dicho desfase, se propone una pequeña modificación al controlador que consiste en establecer una relación de ganancias.

Por otro lado, se propone la introducción de un filtro pasabajas (LPF) de primer orden, derivado de la necesidad de eliminar ruido en la implementación física. Esta modificación introduce un desfase considerable tanto en los picos de resonancia como en los “notches”. En este documento se propone una modificación para minimizar de manera eficiente dicho desfase.

Con el objetivo de conocer las propiedades energéticas del esquema repetitivo propuesto, se estudian las propiedades de pasividad del mismo, concluyéndose que éste es pasivo, y que después de la introducción de amortiguamiento mencionado anteriormente, este se vuelve estrictamente pasivo.

Finalmente, el controlador propuesto así como las modificaciones propuestas, se implementaron digitalmente.





# CONTENTS

<i>List of Acronyms</i> . . . . .	vi
<i>Resumen</i> . . . . .	viii
<i>1. Introduction</i> . . . . .	1
1.1 Overview . . . . .	6
<i>2. Derivation of the Proposed Scheme</i> . . . . .	7
2.1 Preliminaries of multisynchronous transformations and repetitive control	7
2.2 Pole-Zero location of the proposed $6\ell \pm 1$ repetitive scheme . . . . .	14
2.3 First modification: introduction of a limiting gain $K$ . . . . .	16
2.4 Second modification: Introduction of a <i>LPF</i> . . . . .	20
2.5 Preliminaries on Passivity properties of Linear Time discrete time . .	25
2.6 Passivity properties of the hyperbolic tangent compensator . . . . .	27
2.7 Passivity properties of the hyperbolic cotangent compensator . . . . .	28
2.8 Passivity properties of the $6\ell \pm 1$ compensator . . . . .	29
<i>3. Compensation of the phase shift caused by the Practical modifications</i> . .	33

3.1	Eliminating the phase shift caused by the introduction of the damping gain $K$ . . . . .	33
3.2	Reducing the phase shift caused by the introduction of the LPF . . . .	38
4.	<i>Experimental Results</i> . . . . .	45
4.1	Physical Implementation . . . . .	45
4.2	Eliminating the phase shift by proposing different $K_1$ and $K_2$ . . . . .	47
4.3	Compensation of the phase shift caused by the introduction of the LPF	49
5.	<i>Concluding Remarks</i> . . . . .	53
5.1	Future work . . . . .	54
6.	<i>Appendix A</i> . . . . .	55
7.	<i>Appendix B</i> . . . . .	57
8.	<i>Thesis Contributions</i> . . . . .	59

## LIST OF FIGURES

1.1	(a) Block diagram of the conventional repetitive scheme, and (b) Frequency response for $f_0=60$ Hz . . . . .	2
1.2	(a) Block diagram of the hyperbolic cotangent repetitive controller, and (b) Frequency response for $f_0=60$ Hz. . . . .	4
1.3	(a) Block diagram of the hyperbolic tangent repetitive controller, and (b) Frequency response for $f_0=60$ Hz. . . . .	5
2.1	Basic structure of a synchronous-PI based controller. . . . .	8
2.2	Synchronous frame rotations used in a single phase system. . . . .	9
2.3	Synchronous frame rotations used in a three-phase phase system. . . . .	10
2.4	(a) Block diagram of the hyperbolic cotangent controller tuned at $6\omega_0$ , and (b) Frequency response for $f_0=60$ Hz. . . . .	13
2.5	Combined repetitive scheme in a synchronous frame rotating at $\omega_0$ producing resonance peaks at $(6\ell \pm 1)\omega_0$ and notches at $3(\ell + 1)\omega_0$ . . . . .	14
2.6	(a) Block diagram of the proposed $6\ell \pm 1$ repetitive controller, and (b) Frequency response for $f_0=60$ Hz. . . . .	15
2.7	Process of shifting the poles and zeros to the left. . . . .	17
2.8	(a) Block diagram of the proposed $6\ell \pm 1$ repetitive controller, and (b) Frequency Response of the proposed $(6\ell \pm 1)$ repetitive controller for $K \in 0.5, 0.75, 0.95$ and for $f_0=60$ Hz. . . . .	19

2.9	Frequency response of the proposed repetitive controller without (solid line) and with damping (dashed line) gain $K = 0.7$ and $f_0=60$ Hz. . . . .	20
2.10	Block diagram of the proposed repetitive controller including damping gain $K$ and first order <i>LPF</i> . . . . .	22
2.11	Frequency response of the proposed repetitive scheme (solid) without LPF and (dashed) with LPF for $K = 0.9$ , fundamental frequency $f_0=60$ Hz and $\tau=1000$ Hz. . . . .	23
2.12	Nyquist plot of the $6\ell \pm 1$ ( $\ell = 0, 1, 2, \dots$ ), harmonics compensator after LPF modification square marks are placed at real maximums this is at $\omega = (6\ell \pm 1)\omega_0 \pm \left[ \frac{\sqrt{3}(K-1)^2}{\pi} \right] \omega_0$ meanwhile stars are placed at the expected $6\ell \pm 1$ ( $\ell = 0, 1, 2, 3, \dots, \infty$ ). . . . .	24
2.13	Nyquist plot of the $6\ell \pm 1$ compensator after damping gain $K$ modification. Square marks are placed at resonant peaks, that is at $\omega = (6\ell \pm 1)\omega_0 \pm \left[ \frac{\sqrt{3}(K-1)^2}{\pi} \right] \omega_0$ , while star marks are placed at the expected $(6\ell \pm 1)\omega_0$ ( $\ell = 0, 1, 2, 3, \dots, \infty$ ) frequencies. . . . .	31
3.1	Block diagram of the repetitive scheme with $K_1$ and $K_2$ to eliminate phase shift . . . . .	34
3.2	Bode plot of the proposed repetitive scheme with $K_1 = K_2 = 0.7$ (dashed line) and $K_1 = 0.667, K_2 = 0.7$ (solid line). $\Delta_\theta$ represents the difference between same $K$ case and different $K$ 's case. Both cases for $f_0=60$ Hz. . . . .	36
3.3	Nyquist plot of the $6\ell \pm 1$ ( $\ell = 0, 1, 2, \dots$ ), repetitive proposed scheme for different values of $K_1$ and $K_2$ . . . . .	37
3.4	Block diagram of the proposed repetitive scheme with $\Delta\tau_d$ -modification	40

3.5	Frequency response of the repetitive scheme considering $K_1 = 0.75$ and $K_2 = 0.8$ : (dashed) scheme with LPF modification before $\Delta\tau_d$ compensaion; (solid) scheme with LPF after $\Delta\tau_d$ compensation for the phase shift. (top) Magnitude (y-axis dB, x-axis Hz), and (bottom) phase (y-axis deg, x-axis Hz) . . . . .	41
3.6	Frequency response of the repetitive scheme $(6\ell\pm 1)\omega_0$ ( $\ell = 0, 1, 2, 3, \dots, \infty$ ) considering gain $K_2 = 0.8$ : (dashed) before introduction of the LPF. (dotted) after introduction of the LPF, before $\Delta\tau_d$ compensation. (solid) after introduction of the LPF and $\Delta\tau_d$ compensation. (top) Magnitude (y-axis dB, x-axis Hz), and (bottom) phase (y-axis deg, x-axis Hz) . .	42
3.7	Nyquist plot of the $6\ell \pm 1$ ( $\ell = 0, 1, 2, \dots, \infty$ ), harmonic compensator with LPF modification after $\Delta\tau_d$ -compensation and different values for $K_1, K_2$ . . . . .	43
4.1	Texas Instrument DSP. . . . .	46
4.2	Digital implementation of the proposed repetitive scheme. Signal generator provides the input signal for the proposed repetitive scheme. .	46
4.3	Frequency spectrum of the proposed scheme for: <b>(top)</b> $K = 0.9$ and <b>(bottom)</b> $K = 0.75$ . . . . .	47
4.4	<b>(top)</b> Time response $y(t)$ (1 V/div) to <b>(bottom)</b> an input sinusoidal signal $u(t)$ (100 mV/div) with 100 mV of amplitude and 60 Hz of frequency. . . . .	48
4.5	<b>(top)</b> Time response $y(t)$ (1 V/div) to <b>(bottom)</b> an input sinusoidal signal $u(t)$ (100 mV/div) with 100 mV of amplitude and 660 Hz of frequency. . . . .	48
4.6	<b>(top)</b> Time response $y(t)$ (500 mV/div) to <b>(bottom)</b> an input sinusoidal signal $u(t)$ (1 V/div) with 1 V of amplitude and 180 Hz of frequency. . . . .	49

- 
- 4.7 **(top)** Time response (b)  $y(t)$  to an input sinusoidal signal  $u(t)$  with 1 V of amplitude and 60 Hz of frequency (a) with  $K = 0.75$ . **(bottom)** Time response (d)  $y(t)$  to an input sinusoidal signal  $u(t)$  with 1 V of amplitude and 60 Hz of frequency (c),  $K_1 = 0.67$  and  $K_2 = 0.75$ . . . . 50
- 4.8 **(top)** Time response (a)  $y(t)$  to an input sinusoidal signal  $u(t)$  with 1 V of amplitude and 60 Hz of frequency (b) with  $K_2 = 0.9$  before  $\Delta\tau_d$ -compensation. **(bottom)** Time response (c)  $y(t)$  to an input sinusoidal signal  $u(t)$  with 1 V of amplitude and 60 Hz of frequency (d),  $K_1 = 0.88$  and  $K_2 = 0.9$  after  $\Delta\tau_d$ -compensation. . . . . 51
- 4.9 **(top)** Time response (b)  $y(t)$  to an input sinusoidal signal  $u(t)$  with 1 V of amplitude and 300 Hz of frequency (a) with  $K_2 = 0.9$  before  $\Delta\tau_d$  compensation. **(bottom)** Time response (d)  $y(t)$  to an input sinusoidal signal  $u(t)$  with 1 V of amplitude and 300 Hz of frequency (c),  $K_1 = 0.88$  and  $K_2 = 0.9$  after  $\Delta\tau_d$  compensation. . . . . 51
- 4.10 Comparison of the proposed repetitive scheme phase shift with LPF modification (bottom plot) before and (top plot) after  $\Delta\tau_d$ -compensation for  $K_1 = 0.88$  and  $K_2 = 0.9$ . . . . . 52

## 1. INTRODUCTION

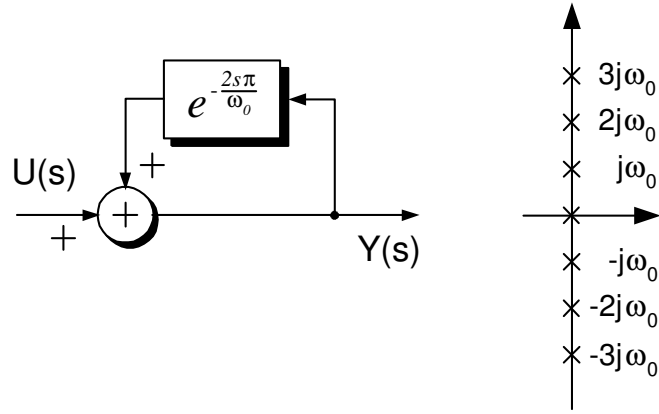
In power electronics applications (i. e. switching power supplies, AC/DC converters, motor speed control, synchronous rectifiers, UPS and active filters) as well as in many communications applications, the tracking or rejection of periodic signals is an issue that commonly arises [1]. Periodic signals can be described as the sum of specific higher harmonics of the fundamental frequency of the power source, which will be referred along the thesis as  $\omega_0$ . Hence the compensation issue above described is addressed also as the harmonic (distortion) compensation issue.

Among the different compensation schemes, repetitive control (see [1], [2], [3]) arises as a simple and practical solution for the harmonic compensation issue providing exact asymptotic output tracking of periodic inputs or rejection of periodic disturbances, and is based on the internal model principle [4]. The internal model principle states that “a controlled output can track a class of reference commands without a steady error if the generator (or the model) of the reference is included in the stable closed loop system”. Therefore, it can be used to provide exact asymptotic output tracking of periodic inputs or to reject periodic disturbances. It is well known that the generator of a sinusoidal signal, i.e., containing only one harmonic component, is a harmonic oscillator, in other words, a resonant filter. Thus, following this idea, if a periodic signal has an infinite fourier series (of harmonics components), then an infinite number of harmonic oscillators are required to track or reject such a periodic signal.

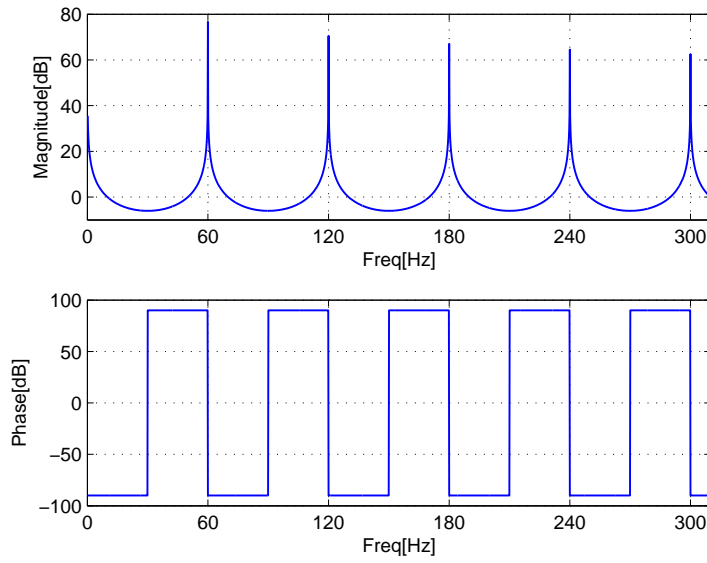
The idea behind the repetitive control approach is that, a simple delay line in a proper feedback array can be used to produce an infinite number of poles and thereby simulate a bank of resonant filters, leading to system dynamics of infinite dimension [5].

First applications of repetitive control were based on the positive feedback scheme





(a)



(b)

Figure 1.1: (a) Block diagram of the conventional repetitive scheme, and (b) Frequency response for  $f_0 = 60$  Hz

[6], [7], [8]. Figure 1.1 shows the block diagram of a repetitive control conventional scheme. The transfer function of this block diagram is given by

$$G(s) = \frac{Y(s)}{U(s)} = \frac{1}{1 - e^{-\frac{2s\pi}{\omega_0}}} \quad (1.1)$$

where  $s = j\omega$  and  $\omega_0$  is the fundamental frequency of the transfer function.

Equation (1.1) generates an infinite number of imaginary poles at every multiple of the fundamental frequency as observed in Figure 1.1(a). The previous statement can be interpreted from its Bode diagram as a bank of resonant peaks tuned at every

single multiple of the  $\omega_0$ , which is settled as  $\omega_0=60$  Hz, and presenting an infinite number of valleys in between two consecutive peaks as observed in Figure 1.1(b).

In [1] a repetitive scheme based on positive feedback-feedforward structure, also called hyperbolic cotangent, was proposed. The feedforward modification produced notches located in between two consecutive poles as observed in Figure 1.2(a). The latter offered the advantage of making the repetitive controller more selective, in the sense that the overlapping in the valleys between two consecutive resonant peaks (as observed in Figure 1.1(b)) was removed by the notches. The transfer function for this repetitive scheme is given by

$$G_1(s) = \frac{Y(s)}{U(s)} = \frac{1 + e^{-\frac{2s\pi}{\omega_0}}}{1 - e^{-\frac{2s\pi}{\omega_0}}} \quad (1.2)$$

It is important to notice that a positive feedback structure may have the disadvantage of compensating for every harmonic, including odd and even harmonics as well as for the dc component. This can be observed in Figure 1.2(b).

Later, a repetitive scheme based on a negative feedback approach with feedforward path was introduced in [1], [9], [10] and [11]. The negative feedback repetitive scheme, also called hyperbolic tangent, is observed in Figure 1.3(a). In contrast to the positive feedback approach, the negative feedback approach was aimed to compensate for the odd harmonics only. It can be observed from Figure 1.3(b) that this scheme generates an infinite number of imaginary poles which can be interpreted as a bank of resonant filters tuned at every odd multiple of the  $\omega_0$ .

The transfer function for the negative feedback-feedforward scheme is given by

$$G_1(s) = \frac{Y(s)}{U(s)} = \frac{1 - e^{-\frac{s\pi}{\omega_0}}}{1 + e^{-\frac{s\pi}{\omega_0}}} \quad (1.3)$$

The last scheme would reduce the possibility of reinjecting unnecessary distortion into the closed loop system.

Depending on the application, there may be interest in the compensation of a selected group of harmonic components. For instance, it is well known that the even harmonic components do not appear regularly in a power system, and that the most

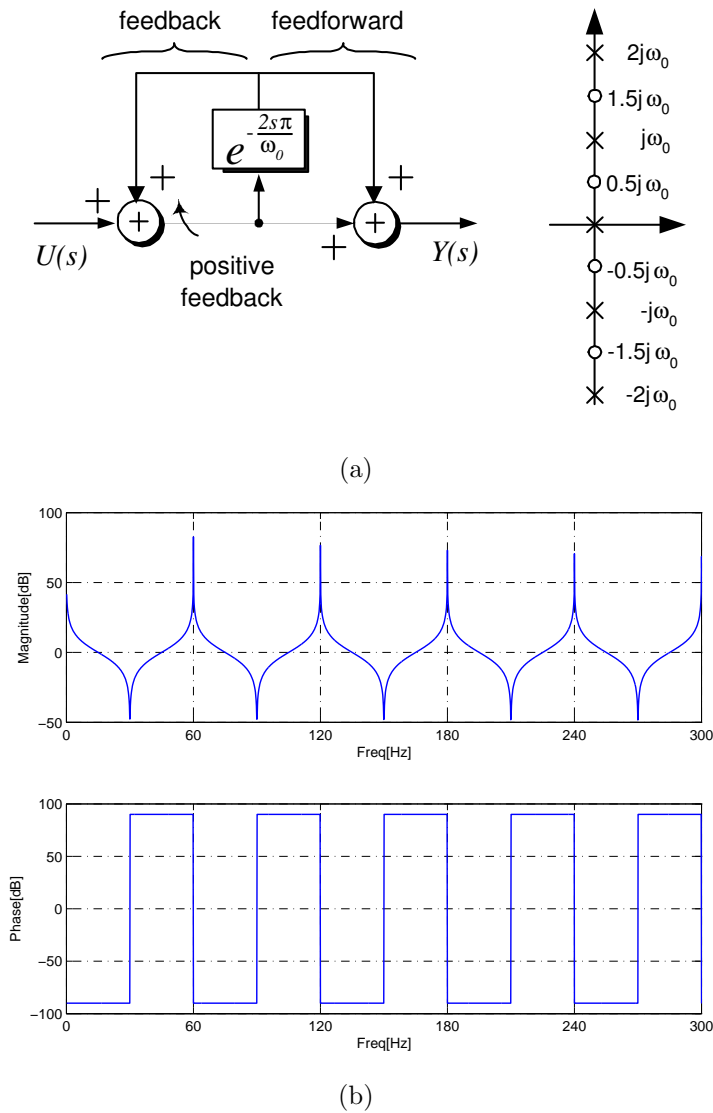


Figure 1.2: (a) Block diagram of the hyperbolic cotangent repetitive controller, and (b) Frequency response for  $f_0=60$  Hz.

commonly found are the odd harmonics. Moreover, it has been observed that among the odd harmonic components, there has been a special interest in industry for the compensation of harmonics multiples  $6\ell \pm 1$  ( $\ell = 0, 1, 2, \dots, \infty$ ) of the  $\omega_0$ , that is, not even harmonics, nor triplet harmonics (multiples of 3). This is due to the fact that many processes in industry involve the use of six pulse converters which produce harmonic components at those specific frequencies [12].

Therefore, even though both the positive and the negative feedback based schemes may apparently solve the harmonics compensation problem, they may lead to more

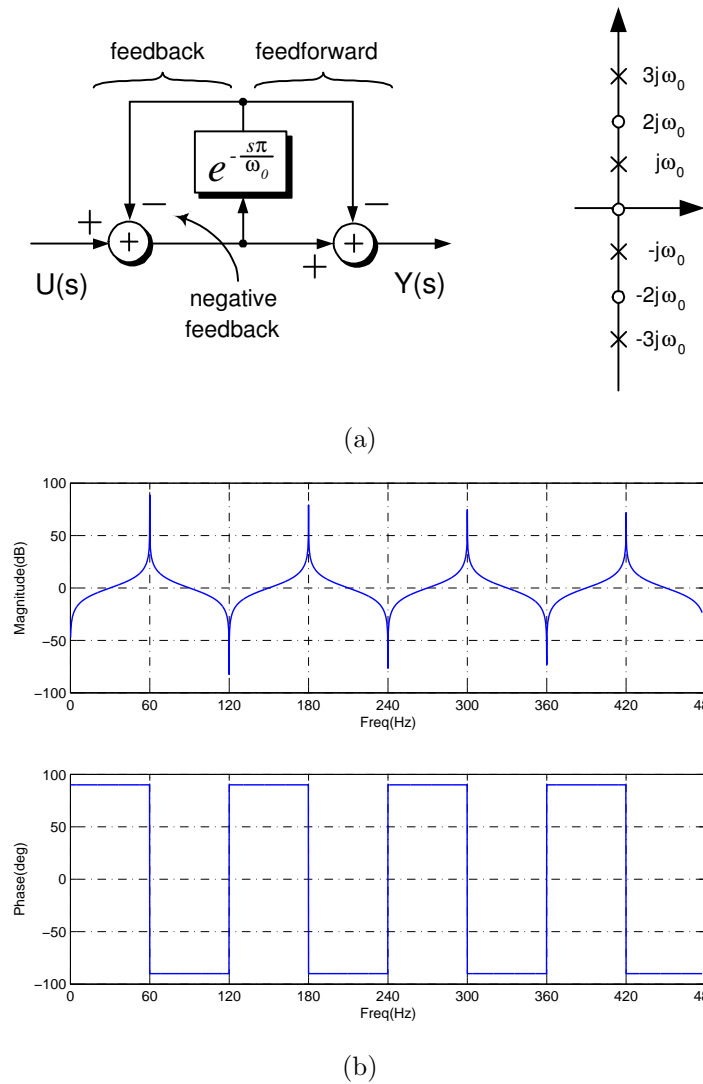


Figure 1.3: (a) Block diagram of the hyperbolic tangent repetitive controller, and (b) Frequency response for  $f_0=60$  Hz.

distortion, as they would tend to amplify, and even reinject, any low level noise having harmonic components on the even and the triplet frequencies. This evidently has the danger of producing responses polluted with such harmonics which were not present before.

The aim of this thesis work is to present a repetitive scheme which would provide the solution to the  $6l \pm 1$  harmonic distortion. The idea behind this proposal is the introduction of a hyperbolic cotangent controller tuned at  $6l\omega_0$  into a multisynchronous transformation. The hypothesis is that after the previous synchronous transformation a frequency shift of  $\pm\omega_0$  will be introduced to the original  $6l\omega_0$  compensator, thereby

generating harmonics at  $6l\omega_0 \pm l\omega_0$ .

## 1.1 Overview

In Chapter 2 the derivation of the proposed repetitive scheme is shown as well as some of its properties. The equivalence between the proposed scheme and a bank of resonant filters is established. It is presented that after introduction of damping to the proposed repetitive scheme, a finite instead of infinite magnitude at resonant peaks is obtained, thus leading to a safer operation. As the repetitive scheme is implemented digitally, a sample frequency process is involved, which leads to the introduction of distortion. Then the introduction of a low pass filter (*LPF*) is proposed. It is observed that due to the introduction of damping and a *LPF*, a phase shift is introduced. Finally, some energetic properties of the proposed repetitive scheme are presented. It is shown that it is passive. Moreover, it is shown that after the damping is introduced the system becomes strictly passive.

In Chapter 3 practical modifications are proposed to the repetitive scheme to eliminate the phase shift due to the introduction of damping and to minimize the phase shift due to the introduction of a *LPF*.

Then in Chapter 4 some experimental results are provided to prove the efficiency of the proposed scheme.

In Chapter 5 some concluding remarks are presented and future work proposals are offered.

## 2. DERIVATION OF THE PROPOSED SCHEME

In this chapter the derivation of the proposed repetitive scheme  $6\ell\omega_0$  is presented which is based on a frequency displacement lemma. After the repetitive scheme is obtained some practical modifications are proposed such as a damping gain and a LPF. Due to the previous modifications a slight phase is introduced.

Passivity properties of the proposed scheme are studied to provide stability properties in closed loop with other passive systems.

### *2.1 Preliminaries of multisynchronous transformations and repetitive control*

The derivation of the proposed scheme is based on the well known modulation (frequency displacement) process that suffers the frequency response of a transfer function when it is pre- and post-multiplied by a frame transformation [13]. This is in agreement with the modulation properties of the Laplace transform [14], since the frame transformations are nothing else than rotations at a given frequency, thus involving the Laplace transform of functions multiplied by sinusoidal terms.

To better understand these ideas, let us consider the very well known technique used in active filters to compensate for the  $\ell$ -th harmonic of the fundamental  $\omega_0$ . This technique consists of the following three steps:

- First, the system variables are transformed to rotating frame quantities at a rotating frequency  $\ell\omega_0$ .
- Second, once in this synchronous frame, the variables are operated by a compensator, where a PI is the most appealed.

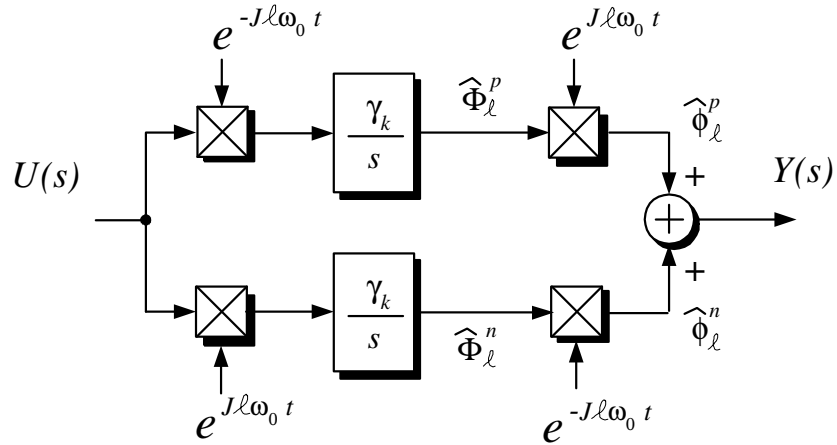


Figure 2.1: Basic structure of a synchronous-PI based controller.

- Third, the compensator outputs are converted back to the stationary reference frame [13], [15].

A PI is usually considered as the compensator since it guarantees zero steady state error of dc disturbances. Figure 2.1 shows the basic structure of a synchronous PI controller [16] including only the integral part. In this figure  $U(s)$  is the input vector,  $Y(s)$  the output vector,  $\hat{\Phi}_\ell^p$  and  $\hat{\Phi}_\ell^n$  are the  $\ell$ -th phasors of the positive and negative sequences, respectively;  $\phi_\ell^p$  and  $\phi_\ell^n$  are the  $\ell$ -th vectors of the positive and negative sequence components; and matrix  $e^{j\ell\omega_0 t}$  is given by

$$e^{j\ell\omega_0 t} = \begin{bmatrix} \cos(\ell\omega_0 t) & -\sin(\ell\omega_0 t) \\ \sin(\ell\omega_0 t) & \cos(\ell\omega_0 t) \end{bmatrix}$$

and

$$e^{-j\ell\omega_0 t} = (e^{j\ell\omega_0 t})^T$$

Notice that, in the synchronous frame, rotating at  $\ell\omega_0$ , the  $\ell$ -th harmonic of a disturbance is assumed to be a dc quantity. Therefore, the PI in such a rotating frame guarantees zero steady state of the  $\ell$ -th harmonic. This type of scheme is referred in the literature as synchronous PI associated to a given rotating frame [16], [17], multiple rotating integrator [18], synchronous-frame harmonic controller

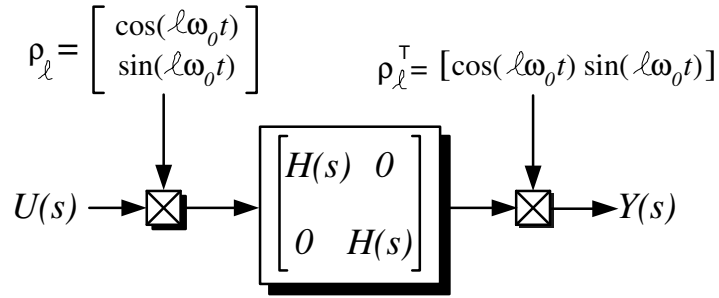


Figure 2.2: Synchronous frame rotations used in a single phase system.

[15], multiple reference frame controller [13], and multi-synchronous PI controllers [19]. The main drawback of this scheme is the cumbersome implementation since it involves two frame transformations, i.e., two rotations for each harmonic component to be compensated.

It has been shown, however, that this complexity, linked to the frame transformations, can be considerably reduced by appealing to the modulation properties of the Laplace transform [20], [21]. Application of such ideas to the synchronous PI, yields the well known resonant plus proportional compensator referred in the literature as resonant regulator [20], [21], PIS compensator [22], [23], stationary-frame generalized integrator [24], multi-resonant controller [19].

A drawback of these schemes is that, a resonant filter was required for each harmonic under compensation, that is, a bank of resonant filters was required for the compensation of several harmonics. In fact it was shown in [25], [26] that by means of suitable rotations it is possible to find the equivalence between the multi-synchronous PI and the multi-resonant controller. To formalize this equivalence the following lemmas can be established, where the first one addresses the single phase case [27]. To better visualize the applicability of this lemma, Figure 2.2 is presented. The second lemma refers to the three phase case, and Figure 2.3 shows the rotations involved in this frame transformation.

**Lemma 2.1** Let

$$x = \text{diag}\{H(p), H(p)\} \rho_\ell u \quad (2.1)$$

$$y = \rho_\ell^\top x \quad (2.2)$$



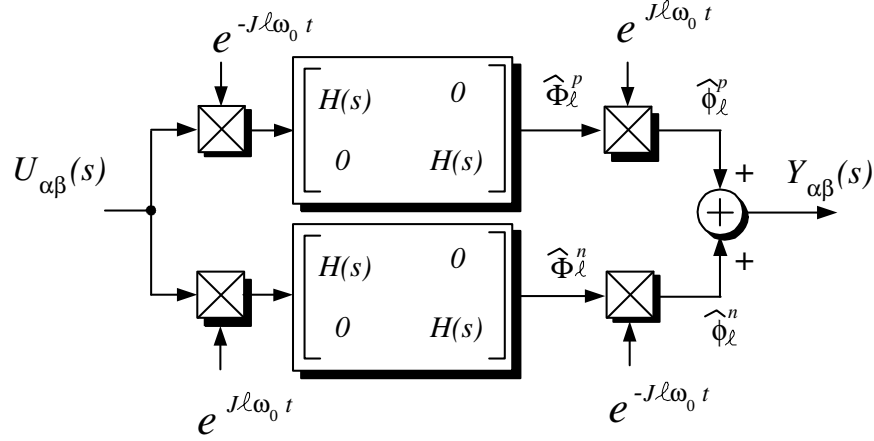


Figure 2.3: Synchronous frame rotations used in a three-phase phase system.

with  $H(p) \in \mathbb{R}(p)$ ,  $u, y \in \mathbb{R}$  and  $\rho_\ell, x \in \mathbb{R}^2$ . Assume

$$\rho_\ell = \begin{bmatrix} \sin(l\omega_0 t) \\ \cos(l\omega_0 t) \end{bmatrix}$$

with  $\omega_0 \in \mathbb{R}_+$  a positive constant and  $\ell$  a positive integer. Then

$$y = \Sigma(p)u \quad (2.3)$$

$$\Sigma(s) = \frac{1}{2}[H(s - j l \omega_0) + H(s + j l \omega_0)] \quad (2.4)$$

□

The proof for this lemma appears in Appendix A.

**Lemma 2.2** Let

$$x_{\alpha\beta}^p = \text{diag}\{H(p), H(p)\}e^{-j l \omega_0} u_{\alpha\beta} \quad (2.5)$$

$$x_{\alpha\beta}^n = \text{diag}\{H(p), H(p)\}e^{j l \omega_0} u_{\alpha\beta} \quad (2.6)$$

$$y_{\alpha\beta} = e^{j l \omega_0} x_{\alpha\beta}^p + e^{-j l \omega_0} x_{\alpha\beta}^n \quad (2.7)$$

$$(2.8)$$

with  $H(p) \in \mathbb{R}(p)$ ,  $u_{\alpha\beta}, y_{\alpha\beta}, x_{\alpha\beta}^p, x_{\alpha\beta}^n \in \mathbb{R}^2$ . Assume

$$e^{j l \omega_0 t} = \begin{bmatrix} \cos(l\omega_0 t) & -\sin(l\omega_0 t) \\ \sin(l\omega_0 t) & \cos(l\omega_0 t) \end{bmatrix}$$

and  $J$  being the skew-symmetric matrix

$$J = \begin{bmatrix} 0 & 1 \\ -1 & 0 \end{bmatrix}$$

with  $e^{-J\ell\omega_0 t} = [e^{J\ell\omega_0 t}]^\top$ ,  $\omega_0 \in \mathbb{R}_+$  a positive constant and  $\ell$  a positive integer. Then

$$y_{\alpha\beta} = \text{diag}\{\Sigma(p), \Sigma(p)\}u_{\alpha\beta} \quad (2.9)$$

$$\Sigma(s) = [H(s - j\ell\omega_0) + H(s + j\ell\omega_0)] \quad (2.10)$$

□

The proof for this lemma appears in Appendix B.

Roughly speaking, the effect of the frame transformation is equivalent to a frequency displacement of the compensator frequency response. For instance, an integrator in the synchronous frame description, i.e.,  $H(s) = 1/s$ , having a pole in the origin, is equivalent to a resonant filter  $\Sigma(s) = \frac{s}{s^2 + \ell^2\omega_0^2}$  having two poles at  $\pm j\ell\omega_0$  in the stationary frame description.

Moreover, if a resonant filter  $H(s) = \frac{s}{s^2 + \ell^2\omega_0^2}$ , having poles at  $\pm j\ell\omega_0$ , is placed inside a rotating frame at a frequency  $\omega_0$ , then the result will be the sum of two resonant filters:

$$\Sigma(s) = \frac{s/2}{s^2 + (\ell + 1)^2\omega_0^2} + \frac{s/2}{s^2 + (\ell - 1)^2\omega_0^2}$$

having poles in  $\pm j(\ell + 1)\omega_0$  and  $\pm j(\ell - 1)\omega_0$  in the stationary frame description. These similar ideas were exploited in [19] to compensate for harmonics 1st, 5th, 7th, 11th and 13th of  $\omega_0$  by using resonant filters tuned at 6th and 12th harmonics of  $\omega_0$  and a PI regulator in a single synchronous frame<sup>1</sup> rotating at the fundamental frequency  $\omega_0$ .

In [1] a positive feedback plus feedforward scheme (also called hyperbolic cotangent) was presented. This scheme produces an infinite number of poles at every single multiple of a given frequency  $\omega_1$ , i.e., located at  $\pm j\ell\omega_1$ , ( $\ell = 0, 1, 2, \dots, \infty$ ), plus an infinite number of zeros located in the midpoint between two consecutive poles, i.e., at  $\pm j\omega_1(2\ell + 1)/2$  (see Figure 1.2). Therefore, if we fix  $\omega_1 = 6\omega_0$  this scheme

<sup>1</sup> The authors use only the  $dq$  reference frame, i.e., only the positive sequence part.

should produce poles located at  $\pm j6\ell\omega_0$ , i.e., resonant peaks at  $6\ell\omega_0$ , and zeros at  $\pm j3(2\ell + 1)\omega_0$ , i.e., notches at  $3(2\ell + 1)\omega_0$ . The expression for this repetitive scheme is given by

$$G(s) = \frac{1 + e^{-\frac{s\pi}{3\omega_0}}}{1 - e^{-\frac{s\pi}{3\omega_0}}} \quad (2.11)$$

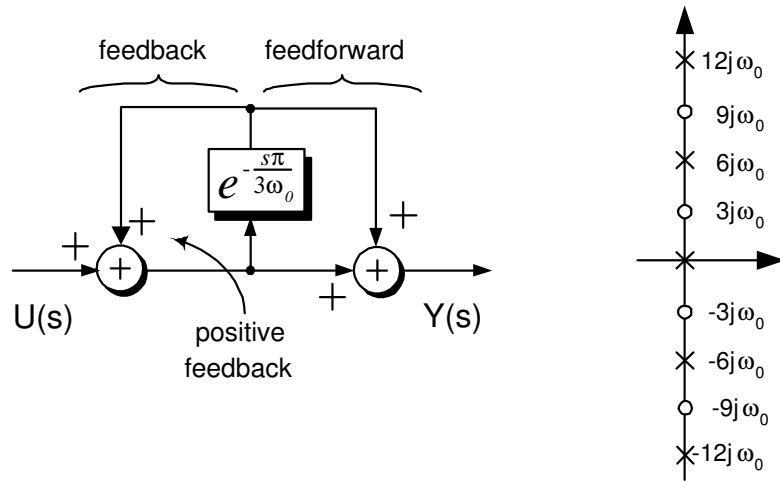
The transfer function (2.11) can be easily implemented as seen in block diagram of Figure 2.4(a), which will generate an infinite number of imaginary poles tuned at  $6\ell\omega_0$ . In the Bode diagram of Figure 2.4 resonant peaks tuned at every  $6\ell\omega_0$  multiples of the fundamental frequency can be observed as predicted. Besides, an infinite number of notches tuned at  $3(2\ell \pm 1)$  are also observed.

Following with the previous ideas (regarding frequency displacement), it is proposed here to place the repetitive scheme (2.11) as the compensator inside a synchronous frame description with frame transformations rotating at  $\omega_0$ . That is, consider  $H(s) = G(s)$  and, for simplicity, consider only the single phase case, then the proposed controller yields the scheme shown in Figure 2.5. This will produce in principle an infinite number of poles located at  $\pm j(6\ell \pm 1)\omega_0$  ( $\ell = 0, 1, 2, \dots, \infty$ ), i.e., an infinite number of resonant peaks will be generated at  $(6\ell \pm 1)\omega_0$  after coming back to the stationary frame description. The combined scheme presented in Figure 2.5 can be further reduced avoiding the frame transformations by simple manipulations as shown below.

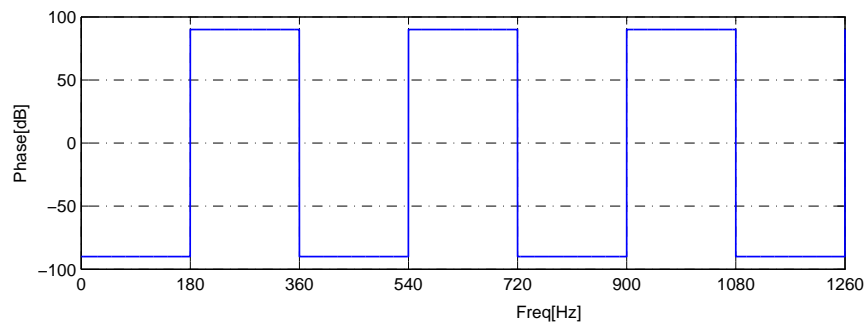
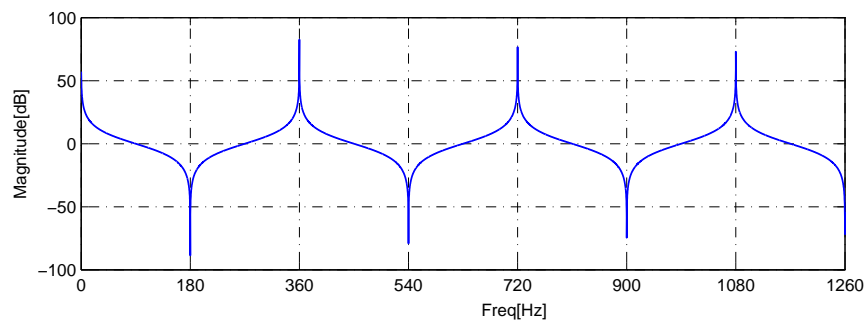
Consider  $H(s) = G(s)$  as given by (2.11), and use expression (2.4) to compute the transfer function, this yields

$$\begin{aligned} \Sigma(s) &= \frac{1}{2} \left( \frac{1 + e^{-(s-j\omega_0)\frac{\pi}{3\omega_0}}}{1 - e^{-(s-j\omega_0)\frac{\pi}{3\omega_0}}} + \frac{1 + e^{-(s+j\omega_0)\frac{\pi}{3\omega_0}}}{1 - e^{-(s+j\omega_0)\frac{\pi}{3\omega_0}}} \right) \\ &= \frac{1 - e^{-\frac{2s\pi}{3\omega_0}}}{1 + e^{-\frac{2s\pi}{3\omega_0}} - e^{-\frac{s\pi}{3\omega_0}} (e^{-\frac{j\pi}{3}} + e^{\frac{j\pi}{3}})} \\ &= \frac{1 - e^{-\frac{2s\pi}{3\omega_0}}}{1 + e^{-\frac{2s\pi}{3\omega_0}} - e^{-\frac{s\pi}{3\omega_0}}} \end{aligned} \quad (2.12)$$

This yields a considerably reduced repetitive scheme which is relatively easy to



(a)



(b)

Figure 2.4: (a) Block diagram of the hyperbolic cotangent controller tuned at  $6\omega_0$ , and (b) Frequency response for  $f_0=60$  Hz.

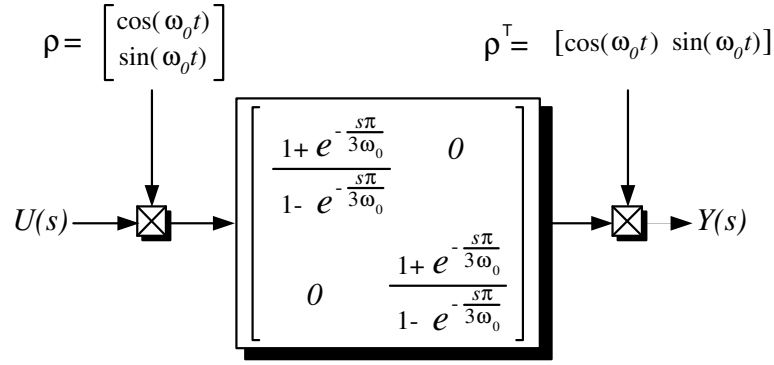


Figure 2.5: Combined repetitive scheme in a synchronous frame rotating at  $\omega_0$  producing resonance peaks at  $(6\ell \pm 1)\omega_0$  and notches at  $3(\ell + 1)\omega_0$ .

implement. It comprises a couple of delays in cascade connection, owning the same time delay arranged in a couple of feedbacks and a feedforward path as shown in Figure (2.6(a)).

## 2.2 Pole-Zero location of the proposed $6\ell \pm 1$ repetitive scheme

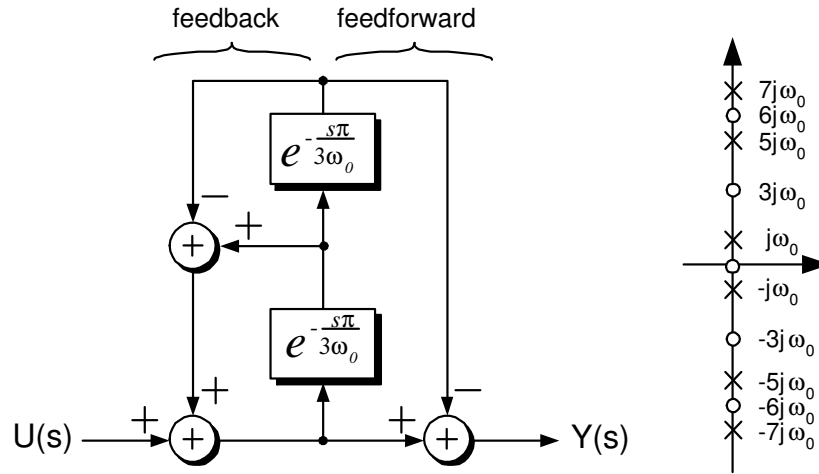
**Proposition 2.3** The  $6\ell \pm 1$  repetitive scheme given by (2.12) has its poles at  $(6\ell \pm 1)\omega_0$  ( $\ell = 0, 1, 2, \dots, \infty$ ), and zeros at  $3\ell\omega_0$  ( $\ell = 0, 1, 2, \dots, \infty$ ). ■

**Proof:** An equivalent expression from (2.12) in terms of hyperbolic functions is obtained as follows

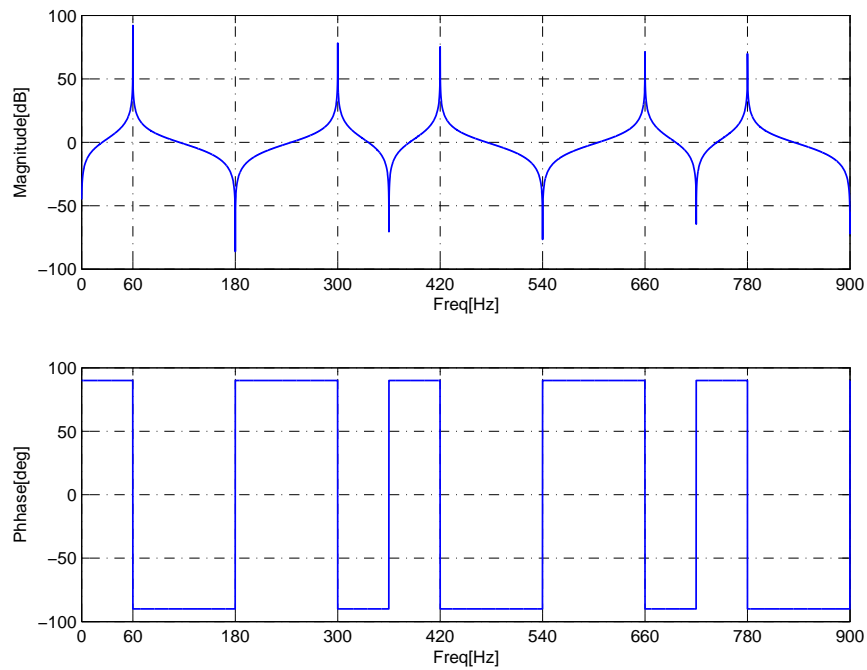
$$\begin{aligned}
 \Sigma(s) &= \frac{1 - e^{-\frac{2s\pi}{3\omega_0}}}{1 + e^{-\frac{2s\pi}{3\omega_0}} - e^{-\frac{s\pi}{3\omega_0}}} = \frac{e^{\frac{s\pi}{3\omega_0}} - e^{-\frac{s\pi}{3\omega_0}}}{e^{\frac{s\pi}{3\omega_0}} + e^{-\frac{s\pi}{3\omega_0}} - 1} \\
 &= \frac{2 \sinh(\frac{s\pi}{3\omega_0})}{2 \cosh(\frac{s\pi}{3\omega_0}) - 1} \tag{2.13}
 \end{aligned}$$

Using properties of the hyperbolic functions [28], an equivalent rational expression can be obtained where numerator and denominator are described in the form of products of binomials as follows

$$\Sigma(s) = \frac{2 \sinh(\frac{s\pi}{3\omega_0})}{2 \cosh(\frac{s\pi}{3\omega_0}) - 1} = \frac{\frac{s\pi}{3\omega_0} \prod_{\ell=1}^{\infty} (\frac{s^2}{(3\ell)^2\omega_0^2} + 1)}{\prod_{\ell=-\infty}^{\infty} (\frac{s^2}{(6\ell+1)^2\omega_0^2} + 1)} \tag{2.14}$$



(a)



(b)

Figure 2.6: (a) Block diagram of the proposed  $6l \pm 1$ repetitive controller, and (b) Frequency response for  $f_0=60$  Hz.

It is easy to see that the transfer function (2.14) contains an infinite number of poles at  $\pm j(6\ell+1)\omega_0$  ( $\ell = 0, 1, 2, \dots, \infty$ ) and  $\pm j(6\ell-1)\omega_0$ . Moreover, it also comprises an infinite number of zeros located at  $\pm j3\ell\omega_0$  as shown in the complex plane in Figure 2.6(a).

As expected, the Bode plot consists of an infinite set of resonant peaks centered at frequencies  $(6\ell \pm 1)$  ( $\ell = 0, 1, 2, \dots, \infty$ ) of  $\omega_0$ , and notches centered at frequencies  $3\ell$  ( $\ell = 0, 1, 2, \dots, \infty$ ) of  $\omega_0$  as shown in Figure 2.6(b). Notice also that the phase shift is zero exactly at those frequencies. Moreover, it can be noticed that the phase shift varies between 90 and -90 degrees.

▽▽▽

It is important to notice that it would be possible, at least in theory, to extend the previous theory for the compensation of  $(12\ell \pm 1)$  harmonics. It would be needed to obtain the transfer function of the hyperbolic cotangent tuned at  $12\omega_0$  and then to apply the modulation lemma to the resulting transfer function. The expected  $\pm\omega_0$  shifting would be obtained. This would result in a delay line modification.

### 2.3 First modification: introduction of a limiting gain $K$

The gain at the resonant frequencies is, in theory, infinite and thus, it may lead to instability problems. To limit the infinite gain at the resonant frequencies, and thus guarantee a safer operation, it is proposed to add damping to all the poles, i.e., to slightly shift them to the left of the imaginary axis [1]. It is important to notice that this modification provides the repetitive scheme with robustness, resulting in a tolerance for a slight shift in the fundamental frequency location.

The shifting process is approached by proposing  $\tilde{\Sigma}(s) = \Sigma(s + a)$ . Applying the shifting to the exponential term in (2.12), it results in  $e^{\frac{-(s+a)\pi}{3\omega_0}} = e^{\frac{-a\pi}{3\omega_0}} e^{\frac{-s\pi}{3\omega_0}}$ . Notice that, this is equivalent to multiply the exponential term by a gain factor  $K$ , where  $K$  would be defined as

$$K = e^{\frac{-a\pi}{3\omega_0}} \quad (2.15)$$

It can be observed from (2.15) that if a gain  $K > 1$  is proposed, the poles move

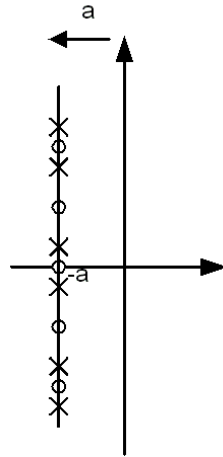


Figure 2.7: Process of shifting the poles and zeros to the left.

to the right, but if  $0 < K < 1$  then they move to the left as shown in Figure 2.7.

The transfer function after this practical modification is given by

$$H(s + a) = \frac{1 - K^2 e^{-2s \frac{\pi}{3\omega_0}}}{1 + K^2 e^{-2s \frac{\pi}{3\omega_0}} - K e^{-s \frac{\pi}{3\omega_0}}} \quad (2.16)$$

The magnitude and phase of transfer function (2.16) are given by

$$|H(j\omega + a)| = \sqrt{\frac{1 + K^4 - 2K^2 \cos(\frac{2\pi}{3\omega_0}\omega)}{1 + K^2 + K^4 - 2(K + K^3) \cos(\frac{\pi}{3\omega_0}\omega) + 2K^2 \cos(\frac{2\pi}{3\omega_0}\omega)}} \quad (2.17)$$

and

$$\theta = -\arctan \left[ \frac{K(1 + K^2 - 4K \cos(\frac{\pi}{3\omega_0}\omega)) \sin(\frac{\pi}{3\omega_0}\omega)}{1 - K^4 + K(-1 + K^2) \cos(\frac{\pi}{3\omega_0}\omega)} \right] \quad (2.18)$$

respectively.

The resonant peaks after the introduction of damping, occur at

$$\omega = \frac{3\omega_0}{\pi} \arccos \left[ \frac{2 + K^2 + 2K^4 - \sqrt{3}\sqrt{1 + K^4 + K^8}}{2(K + K^3)} \right] \quad (2.19)$$

Thus, by substituting (2.19) in (2.17), the magnitude at the resonance peaks (originally of infinite magnitude) reaches a maximum of



$$\sqrt{\frac{6K^2 + 2\sqrt{3}\sqrt{1 + K^4 + K^8}}{3(-1 + K^2)^2}} \quad (2.20)$$

Meanwhile the notches still occur at  $\omega = 3\ell\omega_0$  reaching a magnitude of either

$$m_1 = \frac{1 - K^2}{1 + K + K^2} \quad (2.21)$$

or

$$m_2 = \frac{1 - K^2}{1 - K + K^2} \quad (2.22)$$

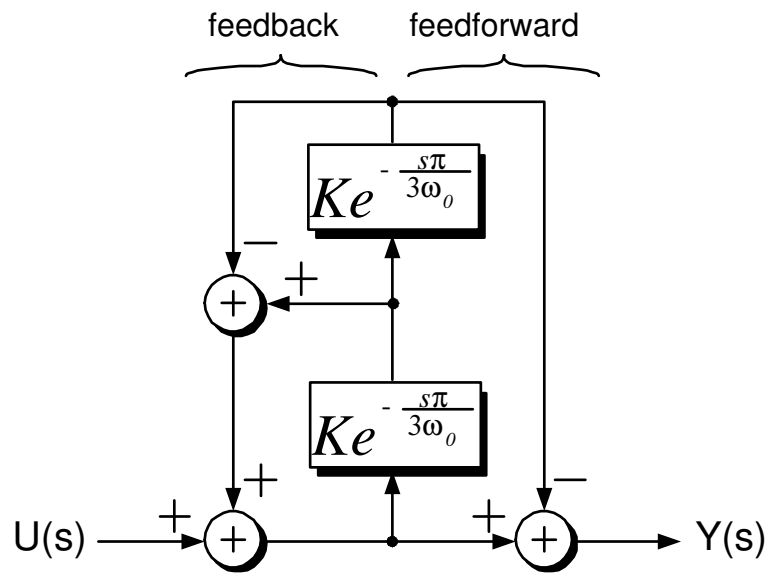
It is important to notice that the new position of the resonant peaks can be approximated using Taylor's series (around  $K = 1$ ), which yields

$$\omega = (6\ell \pm 1)\omega_0 \pm \left[ \frac{\sqrt{3}(K-1)^2}{\pi} \right] \omega_0 \quad (2.23)$$

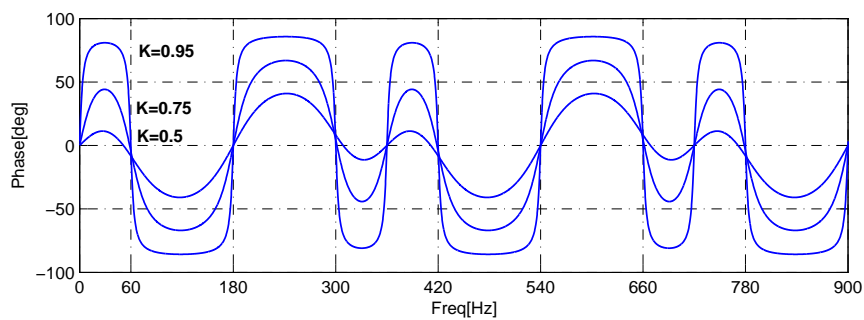
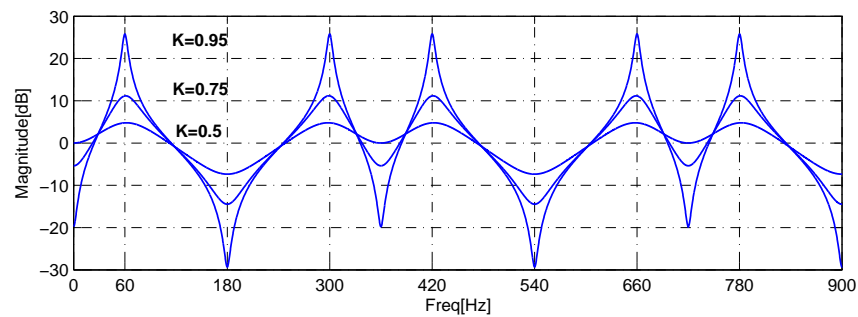
That is, there is a small difference given by  $\frac{\sqrt{3}(K-1)^2}{\pi}\omega_0$  from the expected frequencies  $(6\ell \pm 1)\omega_0$ . Notice that this difference tends to zero as  $K$  gets closer to 1.

Figure 2.8(a) shows the block diagram of proposed scheme after damping  $K$  introduction. Figure 2.8(b) shows the theoretical Bode plots for several values of  $K$  (0.95, 0.75, 0.5), and considering the compensation of harmonics at 60 Hz. In this case, the delay time is fixed to  $\tau_d = \pi/(3\omega_0) = 2.77$  ms. For  $K = 0.95$ , the plot goes from 25.8 dB at the resonant frequencies, to -20 dB or -29.3 dB at the notches. However, if the gain is reduced to  $K = 0.75$ , the corresponding maximum magnitude is 11 dB and for the minimums -5.38 dB or -14.5 dB. A further reduction of  $K$  to  $K = 0.5$  results in maximum magnitudes of 5 dB, and minimum magnitudes of 0 and -7.35 dB.

Figure 2.8(b) clearly shows that, as gain  $K$  decreases, the peak amplitude is reduced while the bandwidth of each peak increases, thus increasing its robustness with respect to frequency variations. However, it can be observed (from the phase plots in Figure 2.8(b)) that the phase shift is not zero at the resonance peaks (due to the effect of gain  $K$  in the transfer function), phase shift is zero at the notches though. It can be noticed that the slight phase shift is introduced only at the resonance



(a)



(b)

Figure 2.8: (a) Block diagram of the proposed  $6l \pm 1$  repetitive controller, and (b) Frequency Response of the proposed  $(6l \pm 1)$  repetitive controller for  $K \in 0.5, 0.75, 0.95$  and for  $f_0=60$  Hz.

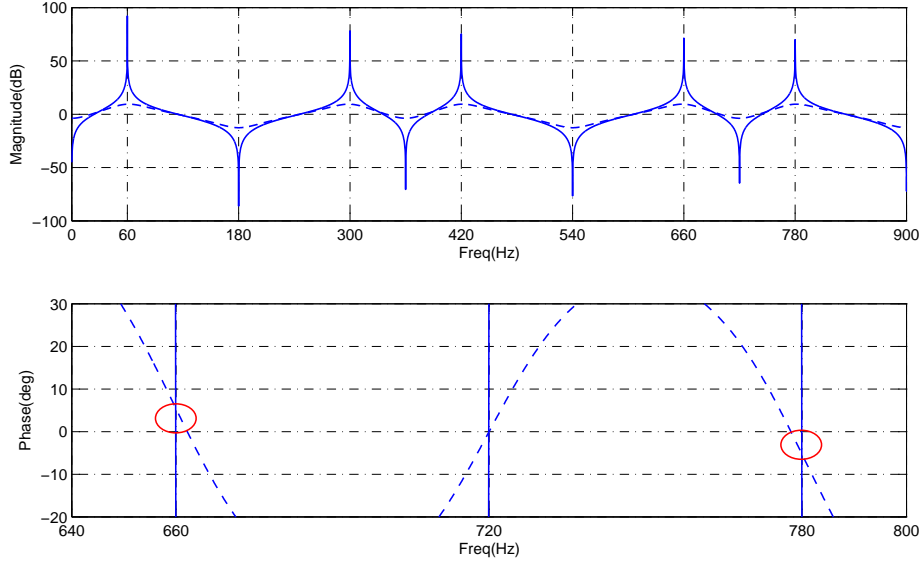


Figure 2.9: Frequency response of the proposed repetitive controller without (solid line) and with damping (dashed line) gain  $K = 0.7$  and  $f_0 = 60$  Hz.

peaks. This phase shift can be approximated using Taylor's series (around  $K = 1$ ) at  $(6l \pm 1)\omega_0$  by

$$\theta = -\frac{(K-3)(K-1)}{2\sqrt{3}} \quad (2.24)$$

Notice that  $\theta$  tends to zero as  $K$  gets closer to 1. Figure 2.9 shows in more detail the phase shift produced by the introduction of the damping gain  $K$  which arises only at the resonance peaks and it is constant. In solid line a damping gain of  $K = 1$  is considered while in dashed line a damping gain of  $K = 0.7$  is considered. It can be observed that, in the case of  $K = 0.7$ , a phase shift equal to 5.36 deg is obtained as shown in Figure 2.9. This phase shift is also obtained by substituting  $K = 0.7$  in (2.24). The possibility to eliminate or at least reduce this phase shift will be explored in next chapter.

#### 2.4 Second modification: Introduction of a LPF

Besides the infinite gain issue, another issue to overcome is the noise introduced by the sampling process, recall that the proposed controller is digitally implemented. As it is well known, digital implementation involves a sampling process which introduces noise into the controller signal. Thus, introduction of a simple Low Pass Filter (*LPF*)

as shown in Figure 2.10 is recommended.

After introduction of the *LPF* of the form  $\frac{1}{\tau s + 1}$ , where  $\tau$  is the cut-off frequency, in the transfer function (2.17), the following transfer function is obtained

$$H_{LPF} = \frac{(\tau s + 1)^2 - K^2 e^{-2s \frac{\pi}{3\omega_0}}}{(\tau s + 1)^2 + K^2 e^{-2s \frac{\pi}{3\omega_0}} - (\tau s + 1) K e^{-s \frac{\pi}{3\omega_0}}} \quad (2.25)$$

Magnitude and phase of the transfer function (2.25) are given by

$$|H_{LPF}| = \sqrt{\frac{N(\omega, K, \tau)}{D(\omega, K, \tau)}} \quad (2.26)$$

where,

$$N(\omega, K, \tau) \triangleq (1 - K^2 + \tau^2 \omega^2)^2 (1 + K^2 + \tau^2 \omega^2 - K \cos(\tau_d \omega) + K \tau \omega \sin(\tau_d \omega))^2 + K^2 (\tau \omega \cos(\tau_d \omega) + \sin(\tau_d \omega))^2 (1 + K^2 + \tau^2 \omega^2 - 4K \cos(\tau_d \omega) + 4K \tau \omega \sin(\tau_d \omega))^2$$

$$D(\omega, K, \tau) \triangleq (1 + K^2 + K^4 + (2 + K^2) \tau^2 \omega^2 + \tau^4 \omega^4 - 2K(1 + K^2 + \tau^2 \omega^2) \cos(\tau_d \omega) + 2K((K - K \tau^2 \omega^2) \cos(2\tau_d \omega) + \tau \omega (1 + K^2 + \tau^2 \omega^2 - 4K \cos(\tau_d \omega)) \sin(\tau_d \omega)))^2$$

and

$$\theta = -\arctan \left[ \frac{K(\tau \omega \cos(\tau_d \omega) + \sin(\tau_d \omega))(1 + K^2 + \tau^2 \omega^2 - 4K \cos(\tau_d \omega) + 4K \tau \omega \sin(\tau_d \omega))}{(1 - K^2 + \tau^2 \omega^2)(1 + K^2 + \tau^2 \omega^2 - K \cos(\tau_d \omega) + K \tau \omega \sin(\tau_d \omega))} \right] \quad (2.27)$$

respectively, where  $\tau_d \triangleq \frac{\pi}{3\omega_0}$ .

The addition of the *LPF* restricts the bandwidth of the controller. However, it may produce some slight inaccuracies as it is observed in Figure 2.11. It is observed that a considerable phase shift appears, and moreover in this case it is different for each  $6\ell \pm 1$  ( $\ell = 0, 1, 2, \dots, \infty$ ) harmonic. The magnitude at the resonant peaks changes also from peak to peak, due to the fact that variable  $\omega$  is multiplying by sinus and cosines functions as observed from (2.26).

Figure 2.11 shows the theoretical Bode plot for transfer function  $H_{LPF}$  for compensation of harmonics at 60 Hz with a delay time fixed to 2.77 ms and a  $K = 0.9$ . In this case a first order low pass filter is considered. The frequency response for the case without the introduction of the LPF is shown in solid line. This plot goes from 19.59 dB at the resonant frequencies to either -23.08 dB or -13.6 dB at the notches.

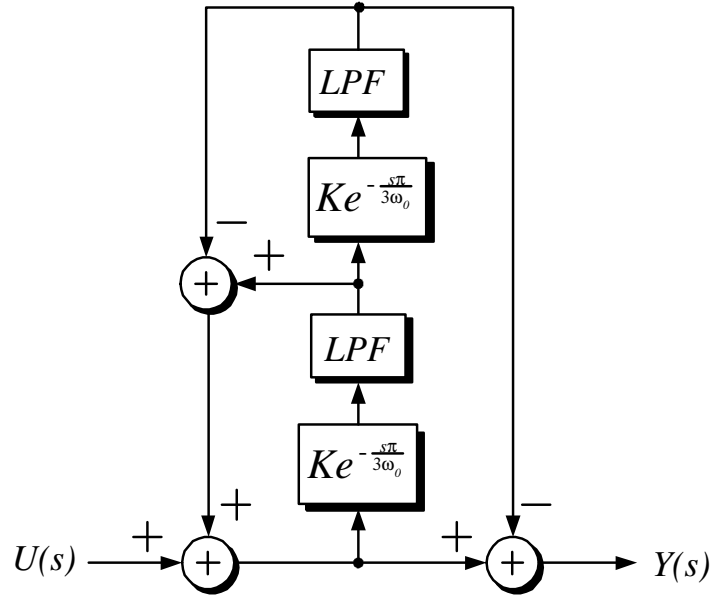


Figure 2.10: Block diagram of the proposed repetitive controller including damping gain  $K$  and first order  $LPF$ .

The frequency response of the transfer function, after the  $LPF$  modification, is shown in dashed line. It can be observed that after the introduction of the  $LPF$ , the resonant peaks have been shifted from the resonant frequencies and a substantial phase shifting has been introduced as well.

On the other hand, Figure 2.12 shows the Nyquist plot after the introduction of the  $LPF$  into the repetitive scheme for different values of  $K$ . Square marks are placed at the resonant peaks, that is at  $\omega = (6\ell \pm 1)\omega_0 \pm \left[ \frac{\sqrt{3}(K-1)^2}{\pi} \right] \omega_0$ , while star marks are placed at the expected  $(6\ell \pm 1)\omega_0$  ( $\ell = 0, 1, 2, 3, \dots, \infty$ ). Numbers on the Nyquist plots regard the harmonic they represent. For example 1 and 1' represent the first harmonic's resonant peak and the first harmonic's magnitude at  $(6\ell \pm 1)\omega_0$  respectively. 5 and 5', 7 and 7', 11 and 11' and 13 and 13', represent the resonant peaks and the magnitudes at  $(6\ell \pm 1)\omega_0$  for  $\ell = 1, 2$  respectively.

It can be observed from the Nyquist plot that the magnitude is different for each harmonic. Besides it can be observed that the magnitude at the resonant peaks presents an important phase from the magnitude at the expected  $(6\ell \pm 1)\omega_0$  ( $\ell = 0, 1, 2, 3, \dots, \infty$ ). Next chapter will explore the possibility of minimizing and even eliminate the phase presented previously.

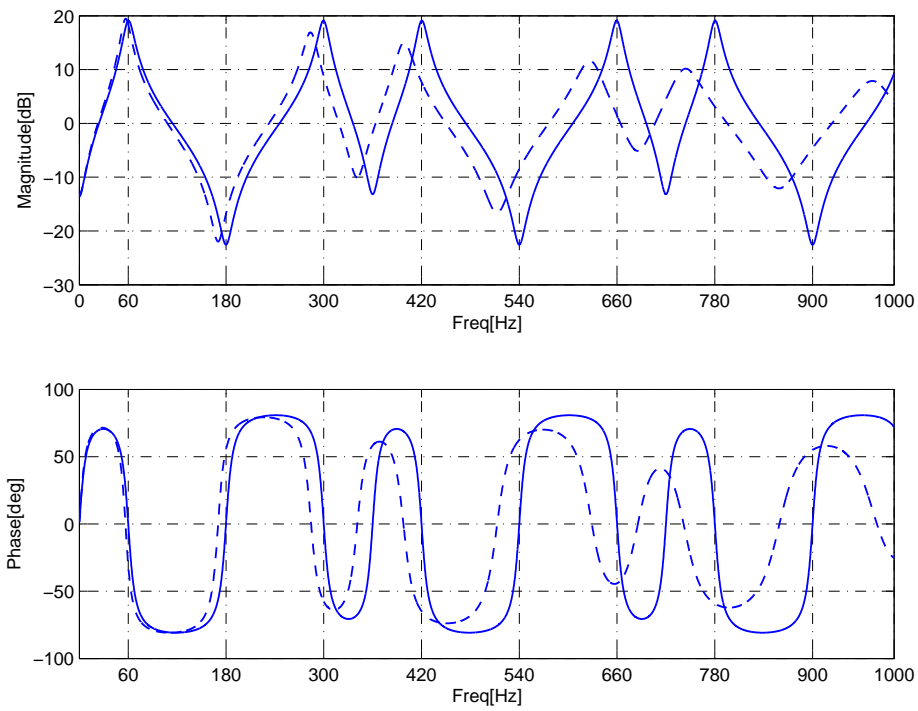


Figure 2.11: Frequency response of the proposed repetitive scheme (solid) without LPF and (dashed) with LPF for  $K = 0.9$ , fundamental frequency  $f_0=60\text{Hz}$  and  $\tau=1000$  Hz.

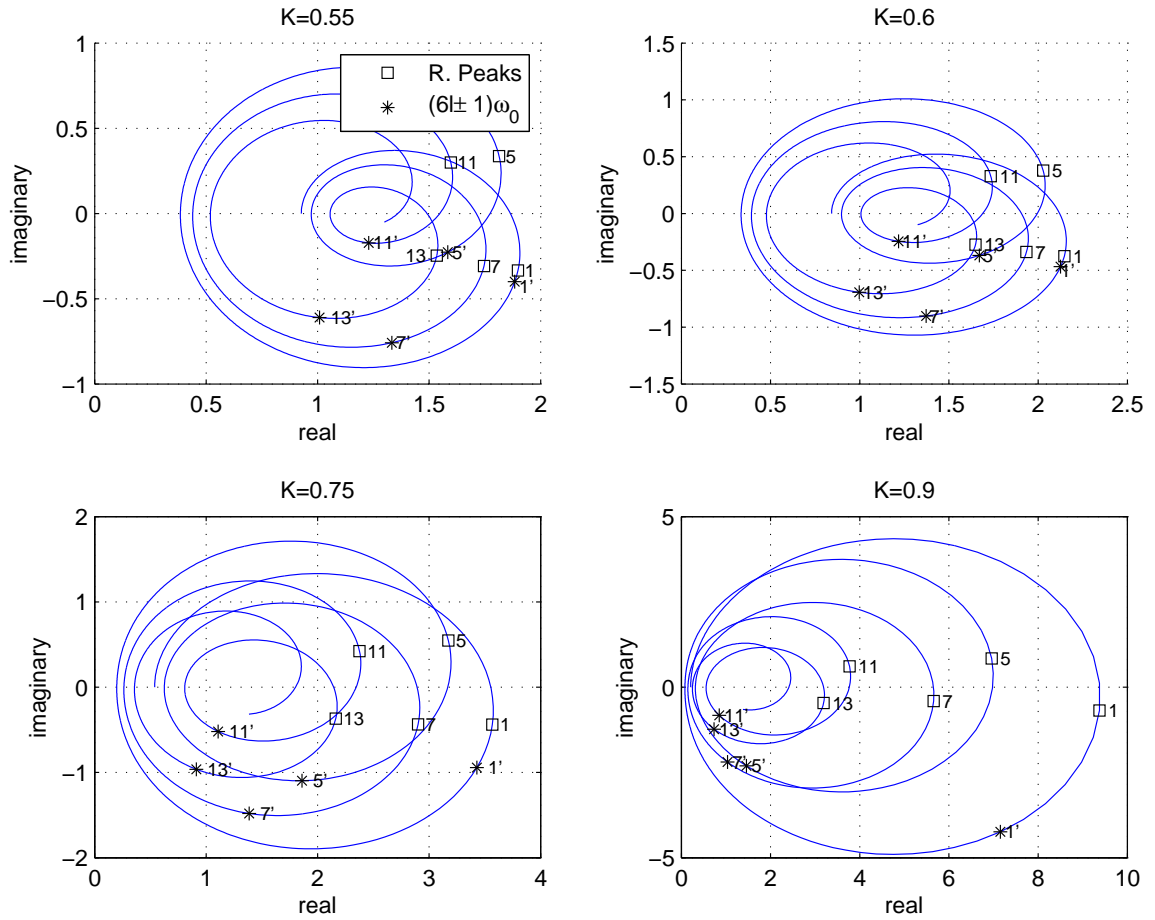


Figure 2.12: Nyquist plot of the  $6\ell \pm 1$  ( $\ell = 0, 1, 2, \dots$ ), harmonics compensator after LPF modification square marks are placed at real maximums this is at  $\omega = (6\ell \pm 1)\omega_0 \pm \left[ \frac{\sqrt{3}(K-1)^2}{\pi} \right] \omega_0$  meanwhile stars are placed at the expected  $6\ell \pm 1$  ( $\ell = 0, 1, 2, 3, \dots, \infty$ ).

Summarizing, as a consequence of these two modifications, i.e., introduction of gain  $K$  and  $LPF$ , two side effects appear: first, resonant peaks and notches are shifted from the corresponding harmonic frequency, and second, a phase shift is introduced. These effects get worst in case that a  $LPF$  is included. In the next chapter some practical modifications are proposed to alleviate the phase-shift issue.

## 2.5 Preliminaries on Passivity properties of Linear Time discrete time

This section studies the passivity properties of the proposed repetitive scheme  $6\ell \pm 1$  as well as the passivity properties of hyperbolic tangent and hyperbolic cotangent controllers. It is shown that these schemes are discrete-time positive real and thus passive. Moreover, after the introduction of damping, it is shown that the proposed repetitive scheme as well as the passivity properties of hyperbolic tangent and hyperbolic cotangent are in fact strictly passive. Passive properties are of great relevance when the proposed repetitive scheme is combined in a closed loop system, as it gives a guarantee of stability.

Before proceeding with the study of the passivity properties of this scheme, it is important to remark that, we are faced with infinite-dimensional delay-differential equations to which the standard tools are not directly applicable. In [29] the authors show that several reported statements of positive-real (PR) discrete-time transfer functions are not completely correct, and presented a lemma that gave the correct conditions for a system to be discrete-time passive, or equivalently discrete-time PR. This lemma is recalled here below for completeness, as well as a lemma taken from [30] which are the basis for the stability study.

**Lemma 2.4 (Discrete-time PR)** Consider an LTI discrete-time system

$$y(k\tau_d) + \sum_{i=1}^{n_D} D_i y(k\tau_d - \ell\tau_d) = \sum_{\ell=0}^{n_N} N_\ell u(k\tau_d - \ell\tau_d)$$

with  $\tau_d \in \mathbb{R}_+$ ,  $k \in \mathbb{Z}_+$ ,  $D_\ell, N_\ell \in \mathbb{R}$ ,  $n_N \leq n_D$ . Assume the associated discrete-time transfer function



$$H(e^{\tau_d s}) = \frac{\sum_{\ell=0}^{n_N} N_\ell e^{-\ell \tau_d s}}{1 + \sum_{i=1}^{n_D} D_i e^{-\ell \tau_d s}} \quad (2.28)$$

is discrete-time PR, that is, it satisfies

- (i)  $H(e^{\tau_d s})$  is analytic in  $|e^{\tau_d s}| > 1$ .
- (ii) All poles of  $H(e^{\tau_d s})$  on  $|e^{\tau_d s}| = 1$  are simple.
- (iii)  $\operatorname{Re}\{H(e^{j\theta})\} \geq 0$  for all  $\theta \in \mathbb{R}$  at which  $H(e^{j\theta})$  exists.
- (iv) If  $e^{j\theta_0}$ ,  $\theta_0 \in \mathbb{R}$  is a pole of  $H(e^{\tau_d s})$ , and if  $r_0$  is the residue of  $H(e^{\tau_d s})$  at  $e^{\tau_d s} = e^{j\theta_0}$ , then  $e^{-j\theta_0} r_0 \geq 0$ .

The system is discrete-time passive, that is, there exists  $\beta_0 \in \mathbb{R}$  such that

$$\sum_{k=0}^N y(k\tau_d)u(k\tau_d) \geq \beta_0$$

for all input sequences  $u(k\tau_d) \in \mathcal{L}_2$  and all  $N \in \mathbb{Z}_+$

□

**Lemma 2.5 (Passivity of continuous-time delayed systems)** Consider an LTI continuous-time system described by the delay equation

$$y(t) + \sum_{i=1}^{n_D} D_i y(t - \ell \tau_d) = \sum_{\ell=0}^{n_N} N_\ell u(t - \ell \tau_d)$$

with  $\tau_d, t \in \mathbb{R}_+$ ,  $D_\ell, N_\ell \in \mathbb{R}$ ,  $n_N \leq n_D$ . Assume the discrete-time transfer function (2.28) is discrete-time PR. Then, the system is passive, that is, there exists  $\beta_1 \in \mathbb{R}$  such that

$$\int_0^t y(\tau)u(\tau)d\tau \geq \beta_1$$

for all input functions  $u(t) \in \mathcal{L}_2$  and all  $t \in \mathbb{R}_+$ .

□

Then the following definition has been extracted from [31] and is used here to prove that the modified proposed scheme is strictly positive real (SPR).

**Definition 2.6**  $H(s)$  is SPR if and only if there exists some  $\varepsilon > 0$  such that  $H(s - \varepsilon)$  is PR.

## 2.6 Passivity properties of the hyperbolic tangent compensator

**Proposition 2.7** The negative feedback-feedforward repetitive scheme given by (1.3) is discrete-time PR and thus passive. ■

**Proof:** Rewriting (1.3) in terms of the delay time  $\tau_d$  yields

$$H(e^{\tau_d s}) = \tanh\left(\frac{\tau_d s}{2}\right) = \frac{1 - e^{-\tau_d s}}{1 + e^{-\tau_d s}} = \frac{e^{\tau_d s} - 1}{e^{\tau_d s} + 1}$$

The partial fraction expansion of this expression gives

$$H(e^{\tau_d s}) = 1 - \frac{2}{e^{\tau_d s} + 1}$$

hence the transfer function satisfies conditions (i) and (ii) of Lemma 2.4. The residue associated with the fixed pole at  $e^{-j\theta_0} = -1$  is  $r_0 = -2$ , and thus condition (iv) is satisfied. Finally, some simple computations prove that,  $Re\{H(e^{j\theta})\} = Re\left\{\frac{j \sin(\theta)}{1 + \cos(\theta)}\right\} = 0$ , thus fulfilling condition (iii). This proves that the hyperbolic tangent scheme is discrete-time PR and, according to Lemma 2.5, it is passive.

▽▽▽

In [1] a gain  $K$  is included to the hyperbolic tangent scheme as follows.

$$\frac{1 - Ke^{-\tau_d s}}{1 + Ke^{-\tau_d s}} \tag{2.29}$$

The aim of this practical modification is to prevent high gains in the resonant peaks and to enhance the robustness with respect to frequency variations. In fact, the peaks, originally of infinite magnitude, reach a maximum magnitude of  $\frac{1+K}{1-K}$  while the notches reach a minimum magnitude of  $\frac{1-K}{1+K}$ .

This modification can also be seen as a frequency shifting process  $\tilde{H}(s) = H(s+a)$  as shown below. By proposing a gain factor  $K = e^{-\tau_d a}$  we obtain

$$\frac{1 - Ke^{-\tau_d s}}{1 + Ke^{-\tau_d s}} = \frac{1 - e^{-\tau_d(s+a)}}{1 + e^{-\tau_d(s+a)}} = \frac{e^{-\frac{\tau_d(s+a)}{2}} - e^{\frac{\tau_d(s+a)}{2}}}{e^{-\frac{\tau_d(s+a)}{2}} + e^{\frac{\tau_d(s+a)}{2}}} = \quad (2.30)$$

$$= \frac{\sinh\left(\frac{\tau_d(s+a)}{2}\right)}{\cosh\left(\frac{\tau_d(s+a)}{2}\right)} = \tanh\left(\frac{\tau_d(s+a)}{2}\right) \quad (2.31)$$

Therefore, if a gain  $K > 1$  is proposed, the poles and zeros move to the right, while if  $0 < K < 1$  is proposed then they move to the left.

The following definition has been extracted from [31] and is used here to prove that the modified proposed scheme is strictly positive real (SPR).

**Definition 2.8** A transfer function  $G(s)$  is SPR if and only if there exists some  $\varepsilon > 0$  such that  $G(s - \varepsilon)$  is PR.

**Proposition 2.9** The modified scheme (2.29) with  $0 < K < 1$  is SPR and thus strictly passive. ■

**Proof:** According to Definition 2.8, it should be proved that, there exists an  $\varepsilon > 0$  such that

$$\frac{1 - Ke^{-\tau_d(s-\varepsilon)}}{1 + Ke^{-\tau_d(s-\varepsilon)}} \quad (2.32)$$

is positive real ( $\in \{PR\}$ ).

First, let us select  $\varepsilon = a$  where  $a = -\tau_d \ln(K)$ . Notice that,  $\varepsilon = a > 0$  as far as  $0 < K < 1$ . Second, consider  $K = e^{-\tau_d a}$  as defined above, which, after direct substitution, reduces expression (2.32) to  $\tanh\left(\frac{\tau_d s}{2}\right)$ . The proof is completed by recalling that,  $\tanh\left(\frac{\tau_d s}{2}\right)$  is PR according to Proposition 2.7.

▽▽▽

## 2.7 Passivity properties of the hyperbolic cotangent compensator

In [32] it is shown that,  $Z(s)$  is PR if and only if  $1/Z(s)$  is PR. And also that,  $Z(s)$  is SPR if and only if  $1/Z(s)$  is SPR. According to this statements and based on the

fact that  $\coth(\cdot) = 1/\tanh(\cdot)$ , it is straightforward to establish the validity of the following corollaries. The time delay required for the implementation of this scheme is given by  $\tau_d = \frac{2\pi}{\omega_0}$ .

**Corollary 2.10** The hyperbolic cotangent scheme given by (1.2) is PR and thus passive.

**Corollary 2.11** The modified scheme

$$\frac{1 + Ke^{-\tau_d s}}{1 - Ke^{-\tau_d s}} \quad (2.33)$$

with  $0 < K < 1$  is SPR and thus strictly passive.

In fact the modified scheme can also be written as  $\coth\left(\frac{\tau_d(s+a)}{2}\right)$  with  $a = -\frac{2}{\tau_d} \ln(K)$ , and taking  $0 < K < 1$  the poles and zeros are shifted to the left of the imaginary axis in the complex plane ( $\text{Re}\{s\} < 0$ ).

## 2.8 Passivity properties of the $6\ell \pm 1$ compensator

**Proposition 2.12** The  $6\ell \pm 1$  repetitive scheme given by (2.12) is discrete-time PR and thus passive. ■

**Proof:** Rewriting (2.12) in terms of the time delay  $\tau_d = \frac{\pi}{3\omega_0}$  (used along this section to simplify the notation) yields

$$H(e^{\tau_d s}) = \frac{1 - e^{-2\tau_d s}}{1 + e^{-2\tau_d s} - e^{-\tau_d s}} = \frac{e^{2\tau_d s} - 1}{e^{2\tau_d s} - e^{\tau_d s} + 1} \quad (2.34)$$

The expansion of this expression gives

$$\begin{aligned} H(e^{\tau_d s}) &= 1 + \frac{e^{\tau_d s} - 2}{e^{2\tau_d s} + 1 - e^{\tau_d s}} \\ &= 1 + \frac{1}{2} \left( \frac{1 + \sqrt{3}i}{e^{\tau_d s} - e^{\frac{i\pi}{3}}} + \frac{1 - \sqrt{3}i}{e^{\tau_d s} - e^{-\frac{i\pi}{3}}} \right) \end{aligned} \quad (2.35)$$

Hence, the transfer function satisfies conditions (i) and (ii) of Lemma 2.4. For (iii) it is found that  $Re\{H(e^{j\theta})\} = Re\left\{\frac{j^2 \sin(\theta)}{-1+2\cos(\theta)}\right\} = 0$ . For the last condition, the two residues are given by  $r_1 = \frac{1}{2} + \frac{\sqrt{3}}{2}i$  and  $r_2 = \frac{1}{2} - \frac{\sqrt{3}}{2}i$ , and the poles corresponding to each residue are  $\theta_1 = \frac{\pi}{3}$  and  $\theta_2 = -\frac{\pi}{3}$ , respectively. Then  $e^{-j\theta_1}r_1 = 1$  and  $e^{-j\theta_2}r_2 = 1$  and the condition is fulfilled. This proves that, the  $6\ell \pm 1$  ( $\ell = 0, 1, 2, 3, \dots, \infty$ ) scheme is discrete-time PR and, according to Lemma 2.5, it is passive.

▽▽▽

As it was presented in chapter 1, a gain  $K$  is included affecting each delay line. The aim of this practical modification is to prevent high gains in the resonance peaks and to enhance the robustness with respect to frequency variations.

This yields the following modified expression

$$H(e^{\tau_d s}) = \frac{1 - K^2 e^{-2\tau_d s}}{1 + K^2 e^{-2\tau_d s} - K e^{-\tau_d s}} \quad (2.36)$$

**Proposition 2.13** The modified scheme (2.16) with  $0 < K < 1$  is SPR and thus strictly passive. ■

**Proof:** According to Definition 2.8, it should be proved that, there exists an  $\varepsilon > 0$  such that

$$\frac{1 - K^2 e^{-2\tau_d(s-\varepsilon)}}{1 + K^2 e^{-2\tau_d(s-\varepsilon)} - K e^{-\tau_d(s-\varepsilon)}} \quad (2.37)$$

is positive real ( $\in \{PR\}$ ).

First, let us select  $\varepsilon = a$  where  $a = -\tau_d \ln(K)$ . Notice that,  $\varepsilon = a > 0$  as far as  $0 < K < 1$ . Second, consider  $K = e^{-\tau_d a}$  as defined above, which, after direct substitution, reduces expression (2.37) to  $\frac{2 \sinh(\tau_d s)}{2 \cosh(\tau_d s) - 1}$ . The proof is completed by recalling that,  $\frac{2 \sinh(\tau_d s)}{2 \cosh(\tau_d s) - 1}$  is PR according to Proposition 2.12.

▽▽▽

Figure 2.13 shows that, the Nyquist plot of scheme (2.36) goes from a flattened circle for  $0 < K < \frac{\sqrt{2}}{10}$  to a cardioid for  $\frac{\sqrt{2}}{10} < K < 2 - \sqrt{3}$ . Then, for  $2 - \sqrt{3} < K < 1$  the Nyquist plot becomes a limaçon that approaches a circle of arbitrarily

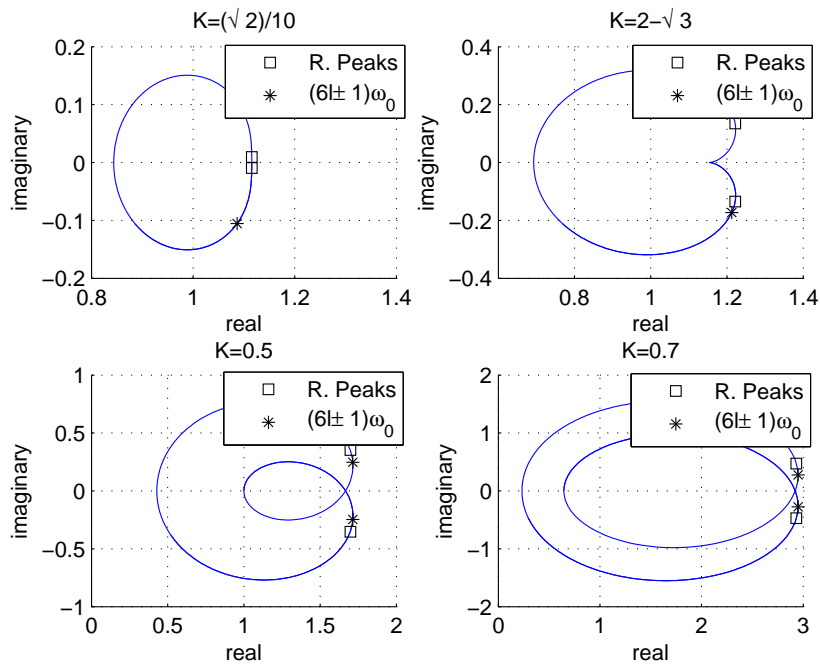


Figure 2.13: Nyquist plot of the  $6\ell \pm 1$  compensator after damping gain  $K$  modification. Square marks are placed at resonant peaks, that is at  $\omega = (6\ell \pm 1)\omega_0 \pm \left[ \frac{\sqrt{3}(K-1)^2}{\pi} \right] \omega_0$ , while star marks are placed at the expected  $(6\ell \pm 1)\omega_0$  ( $\ell = 0, 1, 2, 3, \dots, \infty$ ) frequencies.

large radius as  $K$  gets closer to 1. Square marks are placed at resonant peaks, that is, at  $\omega = (6\ell \pm 1)\omega_0 \pm \left[ \frac{\sqrt{3}}{\pi} \frac{(K-1)^2}{2} \right] \omega_0$ , while star marks are placed at the expected frequencies, that is, at  $(6\ell \pm 1)\omega_0$  ( $\ell = 0, 1, 2, 3, \dots, \infty$ ).

It is clear that the range of interest lies in values of  $K$  slightly smaller than 1, i.e., when the Nyquist plot corresponds to a limaçon. Notice that the Nyquist plot is strictly contained in the right hand side of the complex plane ( $Re\{s\} > 0$ ), as established by (2.21), which is never less than or equal to zero for  $0 < K < 1$ .

### 3. COMPENSATION OF THE PHASE SHIFT CAUSED BY THE PRACTICAL MODIFICATIONS

In this chapter, some practical modifications to the repetitive scheme are proposed to minimize and even to get rid of the phase shift thus compensating in closed loop exactly at the specific  $6\ell \pm 1$  ( $\ell = 0, 1, 2, \dots, \infty$ ) harmonics.

#### *3.1 Eliminating the phase shift caused by the introduction of the damping gain $K$*

As it was previously presented, due to the introduction of positive gain  $K$  in the proposed repetitive transfer function, a slight phase shift appears at the resonant peaks. It was found that the resonant peaks are not exactly placed at  $\omega = (6\ell \pm 1)\omega_0$  ( $\ell = 0, 1, 2, \dots, \infty$ ) but instead they are placed at  $\omega = (6\ell \pm 1)\omega_0 \pm \left[ \frac{\sqrt{3}(K-1)^2}{\pi} \right] \omega_0$  ( $\ell = 0, 1, 2, \dots, \infty$ ). That is, there is a slight difference with respect to the expected frequencies  $\omega = (6\ell \pm 1)\omega_0$  which is given by  $\Delta\omega = \frac{\sqrt{3}(K-1)^2}{\pi} \omega_0$ . Notice that this slight difference reaches zero as  $K$  reaches 1. On the other hand, the phase of transfer function (2.16) at  $\omega = (6\ell \pm 1)\omega_0$  is given by

$$\theta = \mp \arctan \left[ \frac{\sqrt{3}K(-1 + K)}{2 + K + K^2 + 2K^3} \right] \quad (3.1)$$

Notice that expression (3.1) reaches zero as  $K$  reaches 1 but this would lead to infinite gain at resonant peaks. To overcome this issue it is proposed here to utilize two different gains for each delay block, that is, a  $K_1$  to replace the bottom  $K$  and a  $K_2$  for the top  $K$ . After these modifications the block diagram shown in Figure 3.1 is obtained.



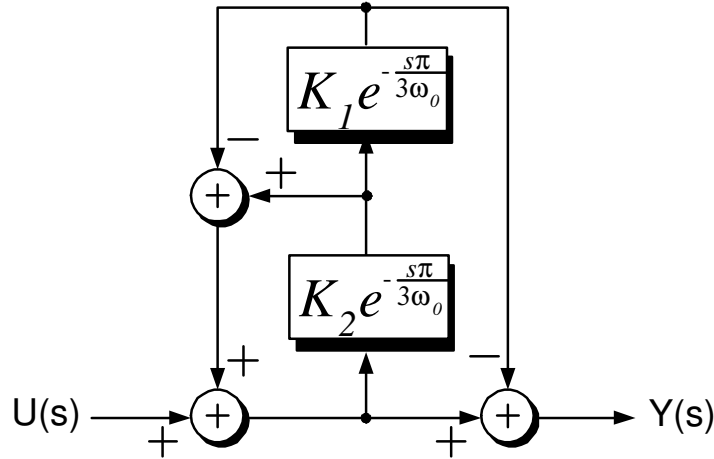


Figure 3.1: Block diagram of the repetitive scheme with  $K_1$  and  $K_2$  to eliminate phase shift

The following transfer function is obtained from the block diagram

$$G(s) = \frac{Y(s)}{U(s)} = \frac{1 - K_1 K_2 e^{-\frac{2s\pi}{3\omega_0}}}{1 + K_1 K_2 e^{-\frac{2s\pi}{3\omega_0}} - K_1 e^{-\frac{s\pi}{3\omega_0}}} \quad (3.2)$$

The phase shift of transfer function (3.2) at  $\omega = (6\ell \pm 1)\omega_0$  ( $\ell = 0, 1, 2, \dots, \infty$ ) is given by

$$\theta = \arctan \left[ \frac{\sqrt{3}K_1(1 - 2K_2 + K_1K_2)}{(-1 + K_1K_2)(2 - K_1 + 2K_1K_2)} \right] \quad (3.3)$$

which is made zero by selecting the gain according to

$$K_1 = 2 - \frac{1}{K_2} \quad (3.4)$$

Thus the previous relationship will ensure phase equal to zero at frequencies  $\omega = (6\ell \pm 1)\omega_0$  ( $\ell = 0, 1, 2, \dots, \infty$ ).

After replacing (3.4) in (3.2) the next transfer function is obtained

$$G_2(s) = \frac{Y(s)}{U(s)} = \frac{1 - (2K_2 - 1)e^{-\frac{2s\pi}{3\omega_0}}}{1 + (2K_2 - 1)e^{-\frac{2s\pi}{3\omega_0}} - (2 - \frac{1}{K_2})e^{-\frac{s\pi}{3\omega_0}}} \quad (3.5)$$

The gain at the resonant peaks for the transfer function (3.5) is given by

$$|G_2(s)| = \frac{1}{\sqrt{2}} \sqrt{\frac{-1 + A + B}{C}} \quad (3.6)$$

where

$$\begin{aligned} A &= 4K_2(1 + 2(-1 + K_2)K_2) \\ B &= \sqrt{-16K_2^6(-1 + 2K_2) + (1 + 4K_2(-1 + 2K_2(1 + (-1 + K_2)K_2)))^2} \\ C &= (-1 + K_2)^2(1 - 2K_2 + 4K_2^2) \end{aligned}$$

Which are located at the following frequencies different from  $(6\ell \pm 1)\omega_0$  ( $\ell = 0, 1, 2, \dots, \infty$ ):

$$\omega = \frac{3}{\pi} \arccos \left[ \frac{1 + D - E}{F} \right] \quad (3.7)$$

where

$$\begin{aligned} D &= -4K_2 + 8K_2^2 - 8K_2^3 + 8K_2^4 \\ E &= \sqrt{-8K_2^6(-2 + 4K_2) + (-1 + 4K_2 - 8K_2^2 + 8K_2^3 - 8K_2^4)^2} \\ F &= 2K_2^2(-2 + 4K_2) \end{aligned}$$

The location of the resonant peaks can be approximated using Taylor's series (around  $K = 1$ ) as  $\omega = (6\ell \pm 1)\omega_0 \mp \left[ \frac{\sqrt{3}}{\pi}(K_2 - 1)^2 \right] \omega_0$ , that is, there is a small difference given by  $\left[ \frac{\sqrt{3}}{\pi}(K_2 - 1)^2 \right] \omega_0$  from the expected frequencies  $(6\ell \pm 1)\omega_0$ . Notice that, this difference approaches zero as  $K$  approaches 1. The gain at  $(6\ell \pm 1)\omega_0$ , ( $\ell = 0, 1, 2, \dots, \infty$ ) is given by  $\frac{K_2}{1 - K_2}$ . There are again two minimums with gains given by  $m_1 = \frac{2(-1 + K_2)K_2}{1 - 2(1 + K_2)}$  and  $m_2 = \frac{2(1 - K_2)K_2}{1 + 2(-1 + K_2)}$ . These minimums occur exactly at frequencies  $3\ell\omega_0$  ( $\ell = 0, 1, 2, \dots, \infty$ ).

**Remark.** It can be observed from  $K_1 = 2 - \frac{1}{K_2}$  that for stability issues,  $K_1$  and  $K_2$ , must lay between 0 and 1. In order to preserve this condition the next restriction shall be fulfilled  $0.5 < K_2 < 1$ .

Figure 3.2 shows the theoretical frequency response of transfer function (2.16) can be observed in dashed line at Figure 3.2 with a fundamental frequency equal to

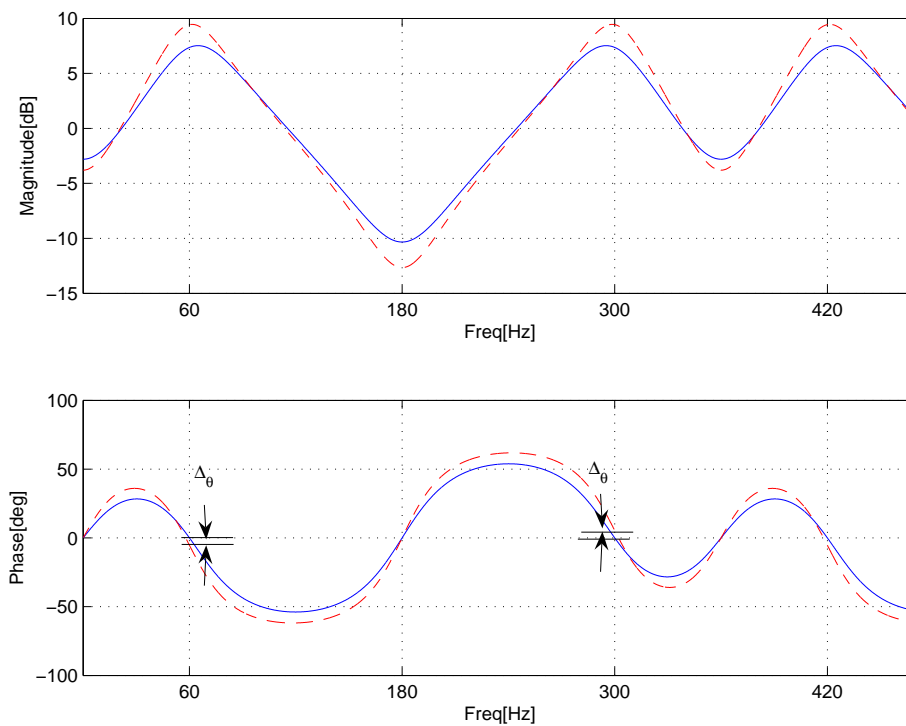


Figure 3.2: Bode plot of the proposed repetitive scheme with  $K_1 = K_2 = 0.7$  (dashed line) and  $K_1 = 0.667, K_2 = 0.7$  (solid line).  $\Delta_\theta$  represents the difference between same  $K$  case and different  $K$ 's case. Both cases for  $f_0=60$  Hz.

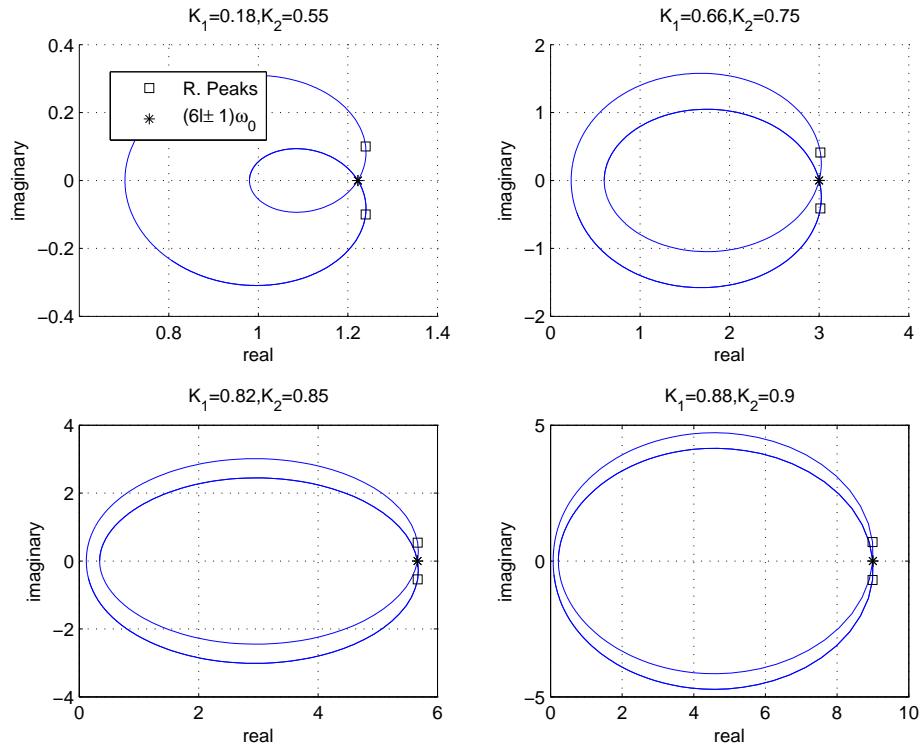


Figure 3.3: Nyquist plot of the  $6\ell \pm 1$  ( $\ell = 0, 1, 2, \dots$ ), repetitive proposed scheme for different values of  $K_1$  and  $K_2$ .

$f_0 = 60$  Hz and the delay time is fixed to  $\tau_d = 2.77$  ms and  $K = 0.7$ . The magnitude goes from 9.45 dB at the resonant frequencies to  $-12.65$  dB or  $-3.8$  dB at the notches.

In solid line the plot for transfer function (3.5) is considered. With a fundamental frequency equal to  $f_0 = 60$  Hz and the delay time is fixed to  $\tau_d = 2.77$  ms and  $K = 0.75$ . this plot goes from 7.5 dB at the resonant frequencies to  $-10.33$  dB or  $-2.8$  dB at the notches.

It can be observed from the phase response of transfer function (2.16) a small phase shift equal to  $\pm 5.36$ . Meanwhile in phase plot of transfer function (3.5) the phase shift has been eliminated at the resonance peaks (due to the effect of the dependent  $K_1$  in the transfer function), and as usual the phase shift is zero at notches. Plots are bounded by 90 and -90 degrees. Later details of the experimental implementation of this modification will be presented.

Figure 3.3 shows the Nyquist diagram for (3.2) this time it can be observed that the phase shift at  $(6\ell \pm 1)\omega_0$  harmonics is zero.

### 3.2 Reducing the phase shift caused by the introduction of the LPF

As it was mentioned previously the addition of a LPF restricts the bandwidth of the controller. However, it may produce some slight inaccuracies. As a consequence of this modification two side effects appear: first, resonant peaks and notches are slightly shifted from the corresponding harmonic frequency, and second, a substantial phase shift appears at the tuned harmonic frequencies.

Let us consider that the *LPF* is introduced in the system of Figure 3.1, that is, using different  $K_1$ ,  $K_2$ , whose transfer function is given by (3.5). The LPF is of the form  $\frac{1}{\tau s + 1}$ , where  $\tau$  is the inverse of the cut frequency. The block diagram of the proposed repetitive scheme after this modification can be seen in Figure 3.4. This modification leads to the next transfer function

$$G_f(s) = \frac{(\tau s + 1)^2 - K_1 K_2 e^{-2\tau_d s}}{(\tau s + 1)^2 + K_1 K_2 e^{-2\tau_d s} - (\tau s + 1) K_1 e^{-\tau_d s}} \quad (3.8)$$

where  $\tau_d = \frac{\pi}{3\omega_0}$

The phase of this transfer function is given by

$$\theta = \mp \arctan \left[ \frac{K_1 (\tau \omega \cos(\tau_d \omega) + \sin(\tau_d \omega)) (1 + K_1 K_2 + \tau^2 \omega^2 - 4K_2 \cos(\tau_d \omega) + 4K_2 \tau \omega \cos(\tau_d \omega))}{(1 - K_2 + \tau^2 \omega^2) (1 + K_1 K_2 + \tau^2 \omega^2 - K_1 \cos(\tau_d \omega) + K_1 \tau \omega \cos(\tau_d \omega))} \right] \quad (3.9)$$

This phase expression is more elaborated than the one in (3.3) due to the introduction of the LPF. It can be observed that the phase shift at the resonant peaks is not constant, since  $\omega$  appears multiplying sinus and cosines functions. Therefore, the phase shift is different for each different harmonic component. Moreover, it can be shown there is not possible combination of  $K_1$  and  $K_2$  to eliminate the phase shift at  $(6\ell \pm 1)\omega_0$  ( $\ell = 0, 1, 2, 3, \dots, \infty$ ) due to the previous arguments. To try to alleviate this issue, it is proposed to introduce an increment  $\Delta\tau_d$  in the time delay which leads to the next transfer function

$$G_{\Delta}(s) = \frac{(\tau s + 1)^2 - K_1 K_2 e^{-2s(\tau_d + \Delta\tau_d)}}{(\tau s + 1)^2 + K_1 K_2 e^{-2s(\tau_d + \Delta\tau_d)} - (\tau s + 1) K_1 e^{-s(\tau_d + \Delta\tau_d)}} \quad (3.10)$$

The objective consist in finding an  $\Delta\tau_d$  such that the phase shift is zeroed at  $(6\ell \pm 1)\omega_0$  ( $\ell = 0, 1, 2, 3, \dots, \infty$ ).

The phase of tranfer function (3.10) is given by

$$\theta_\Delta = -\arctan \left[ \frac{(-1 + 2K_2)(\tau\omega \cos(\theta_d) + \sin(\theta_d))(2K_2 + \tau^2\omega^2 - 4K_2 \cos(\theta_d) + 4K_2\tau\omega \sin(\theta_d))}{(-2 + 2K_2 - \tau^2\omega^2)(K_2(2K_2 + \tau^2\omega^2) + (1 - 2K_2)\cos(\theta_d) + (-1 + 2K_2)\tau\omega \sin(\theta_d))} \right] \quad (3.11)$$

where  $\theta_d = (\tau_d + \Delta\tau_d)\omega$ . It can be shown that the phase shift will equal zero for

$$\Delta\tau_d = \frac{\arctan(\tau\omega)}{\omega} \quad (3.12)$$

Notice, however, that this expression depends on  $\omega$ , and thus, the phase shift can be zeroed at an specific harmonic but not at every harmonic. A solution that solves the problem, at least in average, can be proposed as follows

$$\Delta\tau_d = \frac{1}{\omega_2 - \omega_1} \int_{\omega_1}^{\omega_2} \frac{\arctan(\tau\omega)}{\omega} d\omega \quad (3.13)$$

which computes the average of (3.11) in a range  $[\omega_1, \omega_2]$ . Roughly speaking, the phase shift is minimized in average in this range of frequencies. For instance, if it is desired to compensate the 1st, 5th, 7th, 11th and 13th harmonics of 60 Hz, then the initial and final frequencies could be 0 and 1000 Hz, respectively, since the 1st harmonic starts at 60 Hz and the 13th at 780 Hz. The proposed method leads to valuable results reducing the phase shift on each harmonic frequency considerably as shown in the next simulations.

In what follows, simulations are carried out to highlight the benefits of this  $\Delta\tau_d$ -modification. In these simulations a LPF with cut off frequency equal to 1000 Hz has been considered, and thus, it is convenient to consider,  $\omega_2=2\pi 1000$  rad/s,  $\omega_1=0$  rad/s,  $K_1 = 0.75$  and  $K_2 = 0.8$  have been considered. Evaluation of (3.13) results in  $\Delta\tau_d = -14.8304 \mu\text{s}$ .

Figure 3.5 shows the comparison between the Bode plot with LPF modification before the  $\Delta\tau_d$  compensation (dashed line), and the Bode plot with LPF modification after the  $\Delta\tau_d$  compensation has been enabled (solid line). Notice for instance that, at the 5th harmonic, the phase shift is reduced from  $-35.95$  deg to  $-0.902397$  deg.

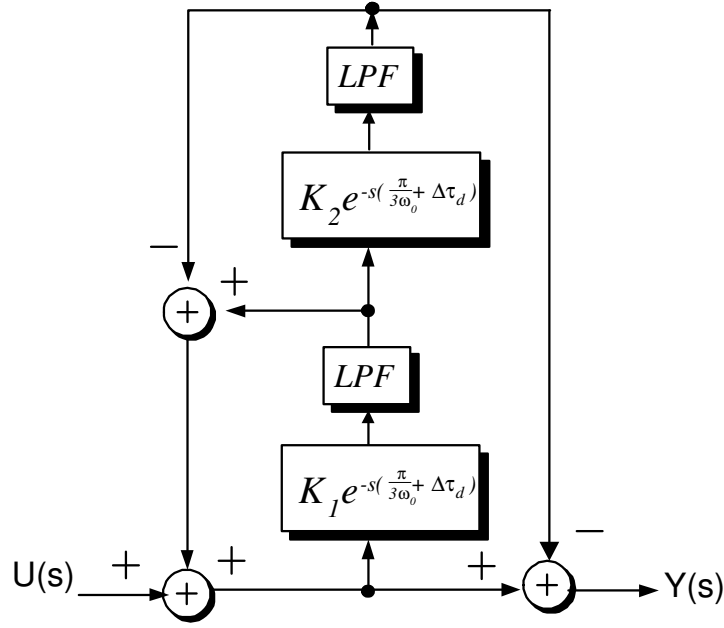


Figure 3.4: Block diagram of the proposed repetitive scheme with  $\Delta\tau_d$ -modification

To show better the advantages of the  $\Delta\tau_d$ -compensation, it can be observed from Figure 3.6 the comparison of three different Bode plots. First, (dashed line) the Bode plot of the proposed repetitive scheme  $(6l \pm 1)\omega_0$  ( $l = 0, 1, 2, 3, \dots, \infty$ ) before introduction of the LPF is shown. Second, (dotted line) the Bode plot of the proposed repetitive scheme  $(6l \pm 1)\omega_0$  ( $l = 0, 1, 2, 3, \dots, \infty$ ) after introduction of the LPF and before  $\Delta\tau_d$  compensation is presented. Finally, (solid line) the Bode plot of the proposed repetitive scheme  $(6l \pm 1)\omega_0$  ( $l = 0, 1, 2, 3, \dots, \infty$ ) after the introduction of the LPF and after enabling the proposed  $\Delta\tau_d$ -compensation is presented. The previous results were obtained for  $f_0=60$  Hz,  $K_1 = 0.75$  and  $K_2 = 0.8$ . It can be observed that the Bode plot after the  $\Delta\tau_d$ -compensation (solid line) follows very close the Bode plot of the controller without the use of a LPF (dashed line), which is the target of the proposed compensation.

Figure 3.7 shows the Nyquist plot for the proposed repetitive scheme after  $\Delta\tau_d$ -compensation to the delay line. Square marks are placed at the resonant peaks, while star marks are placed at the expected  $(6l \pm 1)\omega_0$  ( $l = 0, 1, 2, 3, \dots, \infty$ ). As well as for the case discussed in Chapter 2 (before  $\Delta\tau_d$ -compensation), 1 and 1' represent the first harmonic's resonant peak and the first harmonic's magnitude at  $(6l \pm 1)\omega_0$  respectively. 5 and 5', 7 and 7', 11 and 11' and 13 and 13', represent the resonant

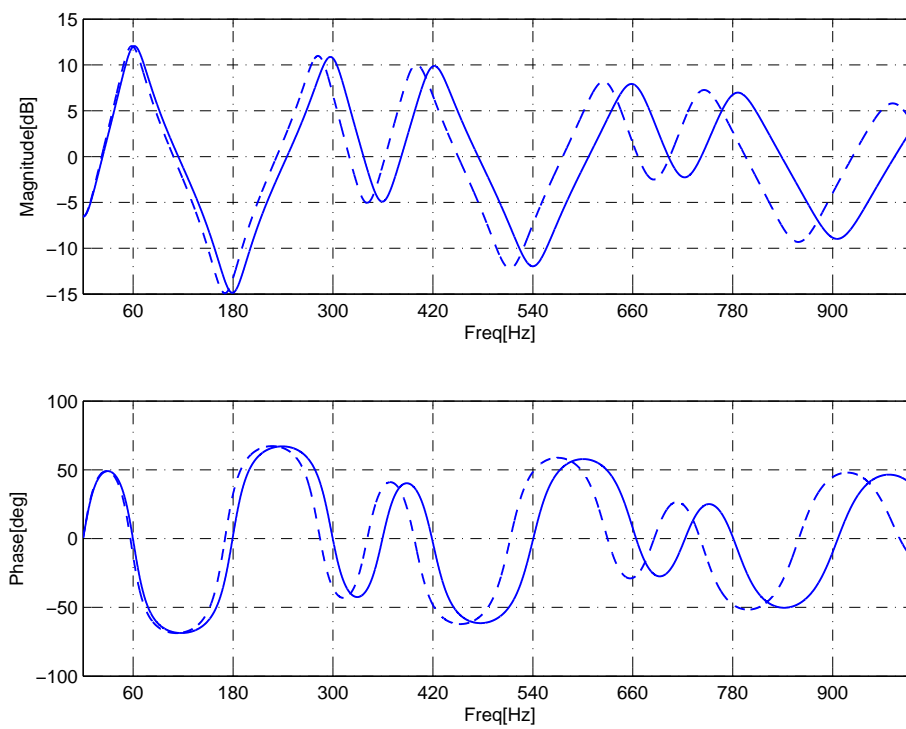


Figure 3.5: Frequency response of the repetitive scheme considering  $K_1 = 0.75$  and  $K_2 = 0.8$  : (dashed) scheme with LPF modification before  $\Delta\tau_d$  compensaion; (solid) scheme with LPF after  $\Delta\tau_d$  compensation for the phase shift. (top) Magnitude (y-axis dB, x-axis Hz), and (bottom) phase (y-axis deg, x-axis Hz)



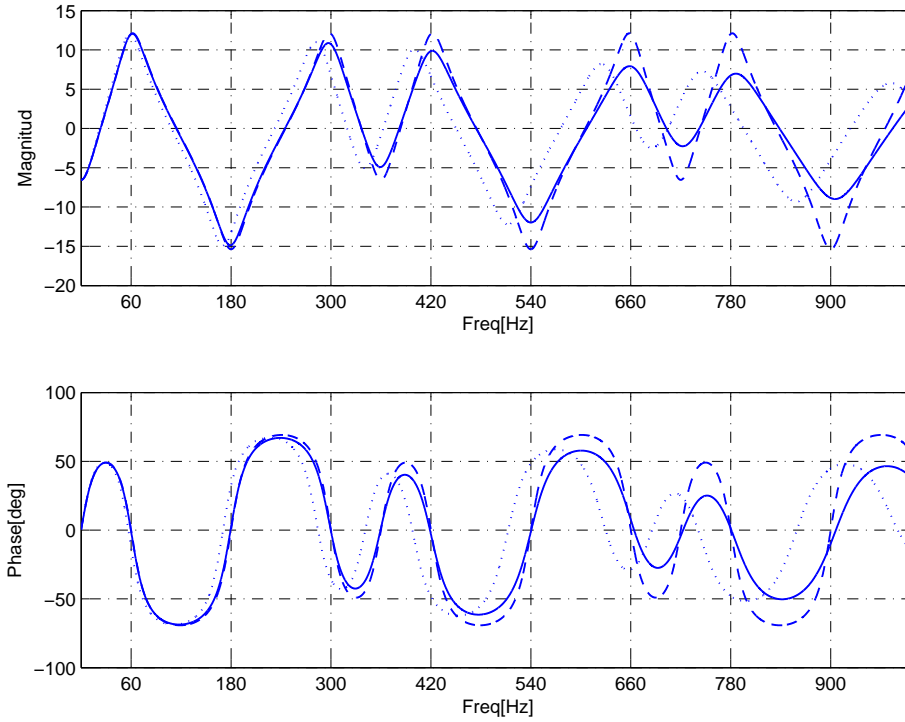


Figure 3.6: Frequency response of the repetitive scheme  $(6\ell \pm 1)\omega_0$  ( $\ell = 0, 1, 2, 3, \dots, \infty$ ) considering gain  $K_2 = 0.8$ : (dashed) before introduction of the LPF. (dotted) after introduction of the LPF, before  $\Delta\tau_d$  compensation. (solid) after introduction of the LPF and  $\Delta\tau_d$  compensation. (top) Magnitude (y-axis dB, x-axis Hz), and (bottom) phase (y-axis deg, x-axis Hz)

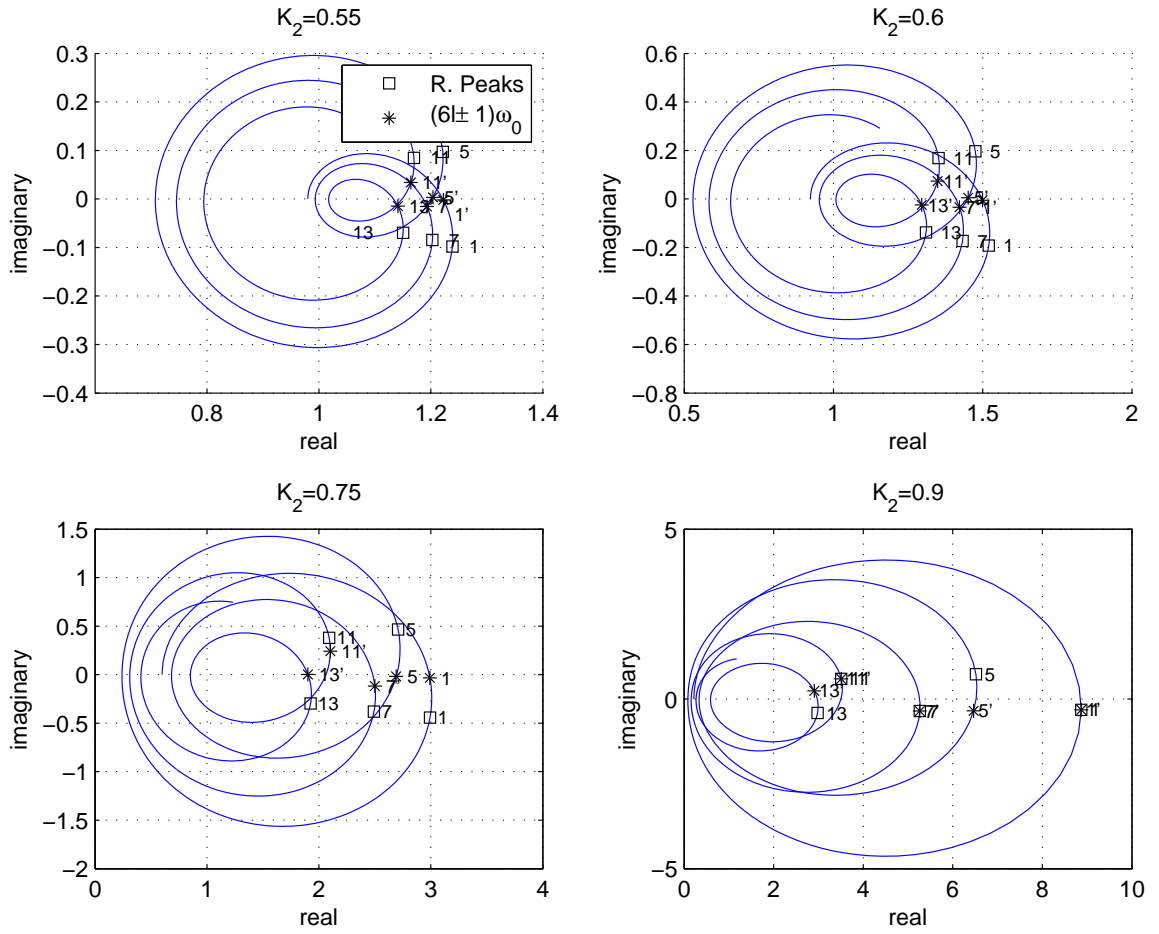


Figure 3.7: Nyquist plot of the  $6\ell \pm 1$  ( $\ell = 0, 1, 2, \dots, \infty$ ), harmonic compensator with LPF modification after  $\Delta\tau_d$ -compensation and different values for  $K_1, K_2$ .

peaks and the magnitudes at  $(6\ell \pm 1)\omega_0$  for  $\ell = 1, 2$  respectively.

It can be observed that after the  $\Delta\tau_d$ -compensation, the phase at  $(6\ell \pm 1)\omega_0$  ( $\ell = 0, 1, 2, 3, \dots, \infty$ ) has been considerably minimized since square marks are very close to star marks.



## 4. EXPERIMENTAL RESULTS

Experimental results are presented in this chapter in order to show the performance of the proposed repetitive scheme  $6\ell \pm 1$  experimentally. Experimental results show that the performance of the proposed repetitive scheme is in accordance with the expected theoretical results.

### 4.1 *Physical Implementation*

A digital implementation of the proposed controller has been developed in the Laboratorio de Procesamiento y Calidad de la Energía for experimental test using the commercial DSP DSP320LF2407 based card from Texas Instruments family as shown in Figure 4.1. The input signal is provided by a signal generator as seen in Figure 4.2, with a sampling rate fixed to  $f_s = 90$  kHz. In fact, the algorithm takes around  $11 \mu\text{s}$ . In this case, the discretization of the delay line is a simple task, and it is necessary only to guarantee a relatively large memory stack where data could be stored to be released after the delay time. The delay time has been fixed to  $\tau_d = \pi/(3\omega_0) = 1/(6f_0) = 1/360 = 2.77$  ms to deal with the  $6\ell \pm 1$  ( $\ell = 0, 1, 2, \dots, \infty$ ) harmonics of  $f_0 = 60$  Hz <sup>1</sup>. A discrete pure delay of the form  $z^{-d}$  has been used to implement the delay line in the repetitive scheme. Therefore, a space of  $d = 250$  memory locations (16 bits each) has been reserved to produce the required delay time, i.e.,  $250/90000 = 2.77$  ms for a sampling frequency of 90 kHz.

The proposed repetitive scheme can also have an analog implementation where the delay lines could be implemented using special purpose integrated circuits such as the BBD circuits, which were thoroughly used in the music industry for reverberation and echo effects [11].

---

<sup>1</sup> For  $f_0 = 50$  Hz a delay of  $\tau_d = 3.33$  ms should be implemented

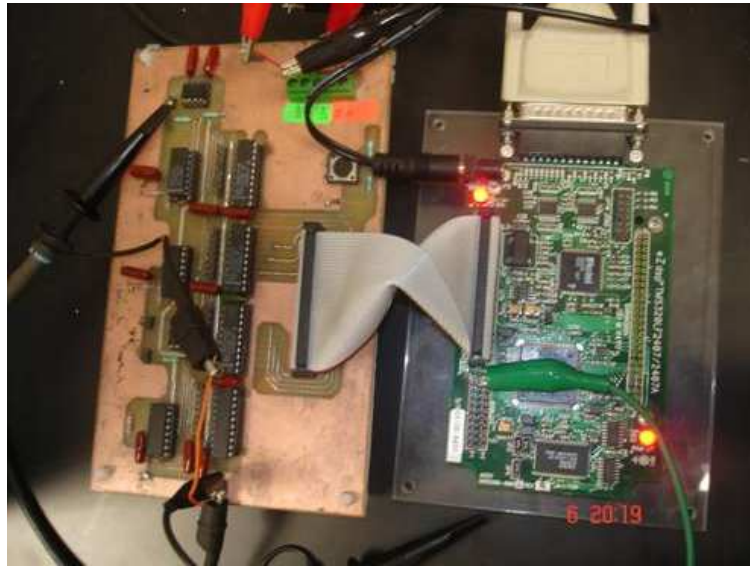


Figure 4.1: Texas Instrument DSP.

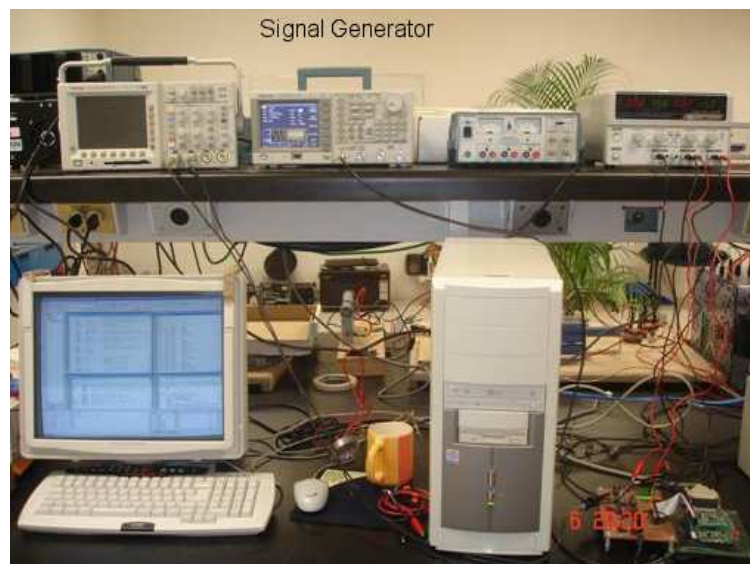


Figure 4.2: Digital implementation of the proposed repetitive scheme. Signal generator provides the input signal for the proposed repetitive scheme.

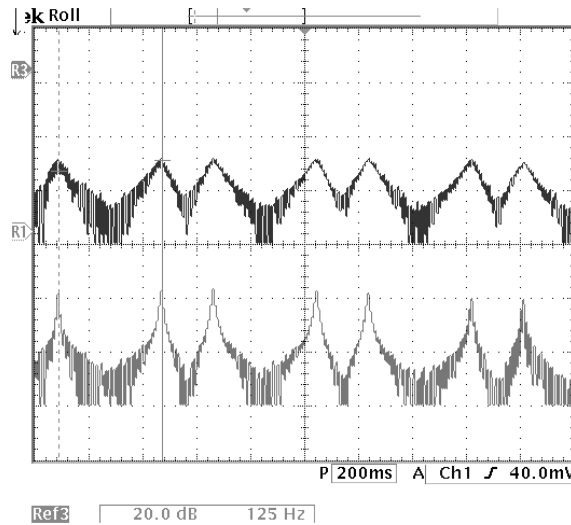


Figure 4.3: Frequency spectrum of the proposed scheme for: **(top)**  $K = 0.9$  and **(bottom)**  $K = 0.75$ .

The experimental frequency response of output  $y(t)$  for the proposed compensator with transfer function (2.16), is shown in Figure 4.3 for  $K=0.75$  and  $K=0.9$ . The plots show that the implemented compensator contains peaks very close to the expected values, i.e., harmonics of 60 Hz. Figure 4.4 shows the time responses to an input sinusoidal signal with 100 mV of amplitude and 60 Hz of frequency (top). It can be observed that the output  $y(t)$  (bottom) reaches amplitude of 950 mV, which corresponds to 19.55 dB of gain, which is very close to that obtained theoretically (19.59 dB). Figure 4.5 show the output for the corresponding 11th harmonic, 660 Hz.

Figure 4.6 shows the responses to an input sinusoidal signal with amplitude 1 V and frequency 180 Hz (top), that is, at the third harmonic, which coincides with the frequency of the notch located between peaks of 60 Hz and 300 Hz. The output  $y(t)$  (bottom) reaches a magnitude of 100 mV which makes a gain of -20dB, which is close to the theoretical result. Notice that, in this plot, the scale of the output signal has been reduced to show its final shape.

## 4.2 Eliminating the phase shift by proposing different $K_1$ and $K_2$

The experimental time response of output  $y(t)$ , for the proposed compensator for transfer functions (2.16) and (3.5), is shown in Figure 4.7. The curve named “b” in

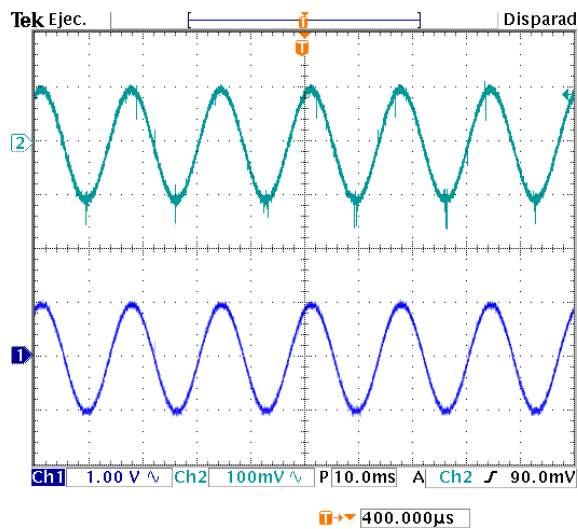


Figure 4.4: **(top)** Time response  $y(t)$  (1 V/div) to **(bottom)** an input sinusoidal signal  $u(t)$  (100 mV/div) with 100 mV of amplitude and 60 Hz of frequency.

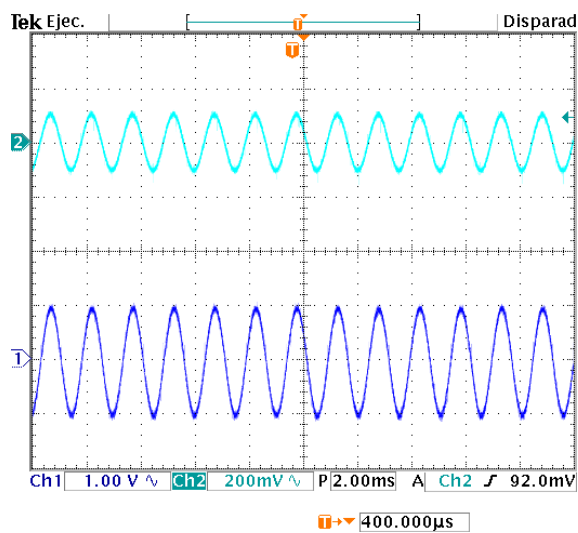


Figure 4.5: **(top)** Time response  $y(t)$  (1 V/div) to **(bottom)** an input sinusoidal signal  $u(t)$  (100 mV/div) with 100 mV of amplitude and 660 Hz of frequency.

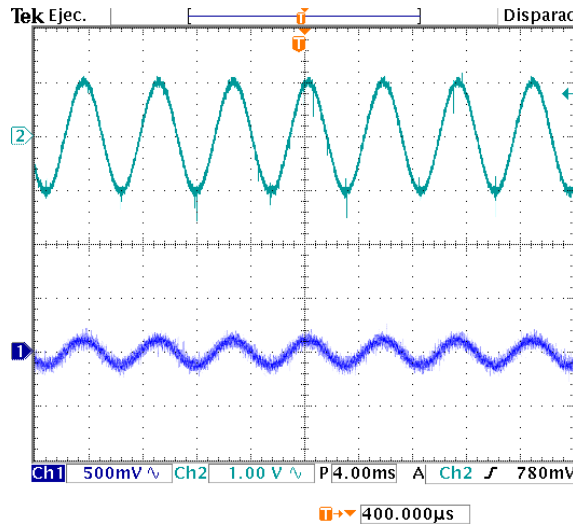


Figure 4.6: **(top)** Time response  $y(t)$  (500 mV/div) to **(bottom)** an input sinusoidal signal  $u(t)$  (1 V/div) with 1 V of amplitude and 180 Hz of frequency.

the top, shows the time response to the input signal (a) with 100 mV of amplitude and 60 Hz of frequency, and considering a  $K = 0.75$ . Drawing the input and output plots, one over the other allows us to observe the small phase-shift caused by the introduction of a unique  $K$ . The sketched phase shift coincides with the theoretical phase shift result.

As previously discussed, the phase observed in the top plot is eliminated by proposing different  $K_1$  and  $K_2$  based on condition (3.4). The d named curve in the bottom plot shows the time response to an input signal (c) with 100 mV of amplitude,  $f_0 = 60$  Hz,  $K_2 = 0.75$  and  $K_1 = 0.67$ . Notice that, as it was expected, the phase shift equals zero. Moreover, the output magnitude at this frequency is slightly reduced from 11.12 dB to 9.54 dB, which coincides with the results predicted by theory.

### 4.3 Compensation of the phase shift caused by the introduction of the LPF

It is proposed in Chapter 3 that for the compensation of the phase shift caused by the introduction of the LPF, only an increment in the delay time is required. Recalling (3.13) and by proposing  $f_2 = 1000$  Hz and  $f_1 = 0$  Hz the value  $\Delta\tau_d = -14.8304 \mu\text{s}$  is obtained. This  $\Delta\tau_d$  value is equivalent to take off 3 memory spaces from the original



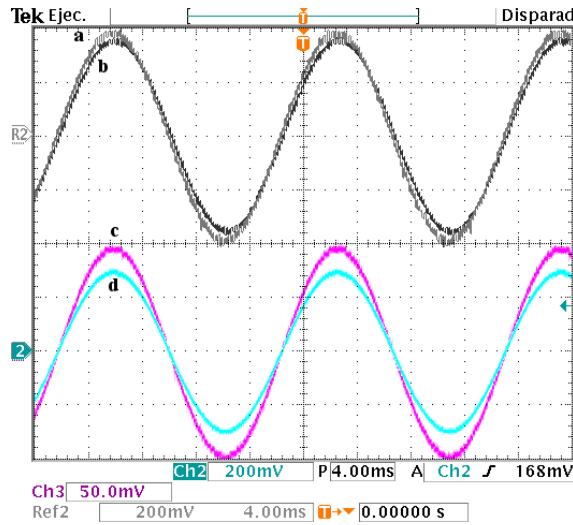


Figure 4.7: **(top)** Time response (b)  $y(t)$  to an input sinusoidal signal  $u(t)$  with 1 V of amplitude and 60 Hz of frequency (a) with  $K = 0.75$ . **(bottom)** Time response (d)  $y(t)$  to an input sinusoidal signal  $u(t)$  with 1 V of amplitude and 60 Hz of frequency (c),  $K_1 = 0.67$  and  $K_2 = 0.75$ .

memory stack of 500 memory locations. Sampling frequency is fixed at to 88800 Hz.

Figure 4.8 shows the two time responses to an input sinusoidal signal with 100 mV of amplitude and 60 Hz of frequency. This time the first order LPF has been introduced with a cut frequency equal to 1000 Hz. In the top, the input signal  $u(t)$  (a) and the output response  $y(t)$  (b) are shown. It can be observed that a considerable phase-shift of about -30 deg is introduced as predicted by theory. In the bottom, for the same input (c), the response (d) is shown. Notice that the phase shift has been reduced to about -3.6 degrees due to the addition of the increment  $\Delta\tau_d$  in the delay line. In this test a  $K_2 = 0.9$  and  $K_1 = 0.88$  were chosen.

A similar experiment as before, considering this time an input signal of 300 Hz is presented in Figure 4.9. This figure shows the two time responses to an input sinusoidal signal with 100 mV of amplitude and 300 Hz of frequency. In the top, the input signal  $u(t)$  (a) and the output response  $y(t)$  (b) are shown. As before a first order LPF has been introduced with a cut-off frequency equal to 1000 Hz. It can be observed that a considerable phase shift of about -57.6 deg is obtained as predicted by theory. And in the bottom, it can be observed that after the introduction of  $\Delta\tau_d$  in the delay line the phase shift is minimized to -2.8 degrees. In both cases  $K_1 = 0.88$  and  $K_2 = 0.9$  is considered.

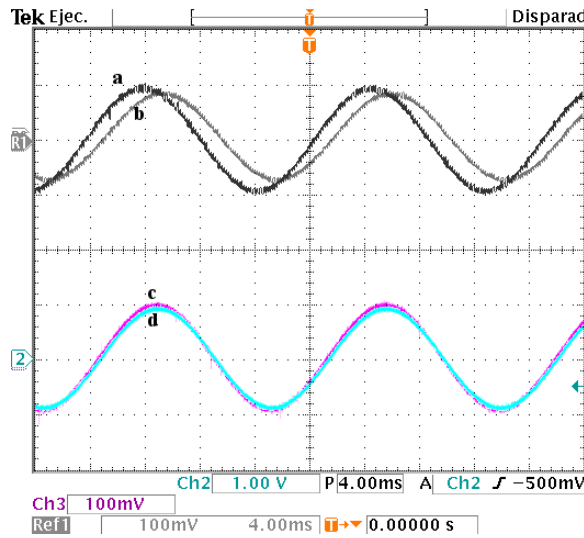


Figure 4.8: **(top)** Time response (a)  $y(t)$  to an input sinusoidal signal  $u(t)$  with 1 V of amplitude and 60 Hz of frequency (b) with  $K_2 = 0.9$  before  $\Delta\tau_d$ -compensation. **(bottom)** Time response (c)  $y(t)$  to an input sinusoidal signal  $u(t)$  with 1 V of amplitude and 60 Hz of frequency (d),  $K_1 = 0.88$  and  $K_2 = 0.9$  after  $\Delta\tau_d$ -compensation.

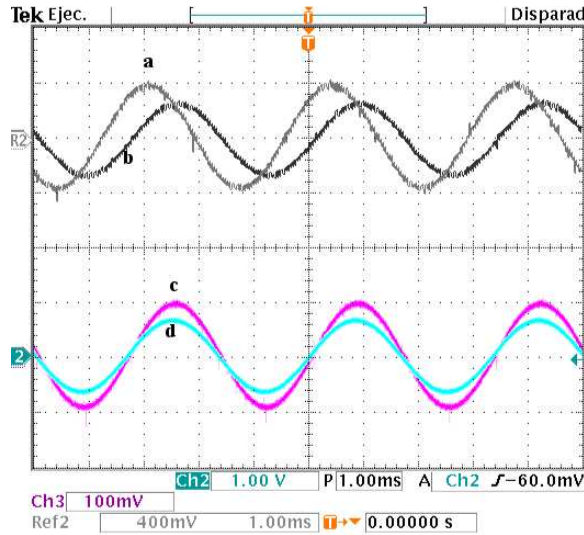


Figure 4.9: **(top)** Time response (b)  $y(t)$  to an input sinusoidal signal  $u(t)$  with 1 V of amplitude and 300 Hz of frequency (a) with  $K_2 = 0.9$  before  $\Delta\tau_d$  compensation. **(bottom)** Time response (d)  $y(t)$  to an input sinusoidal signal  $u(t)$  with 1 V of amplitude and 300 Hz of frequency (c),  $K_1 = 0.88$  and  $K_2 = 0.9$  after  $\Delta\tau_d$  compensation.

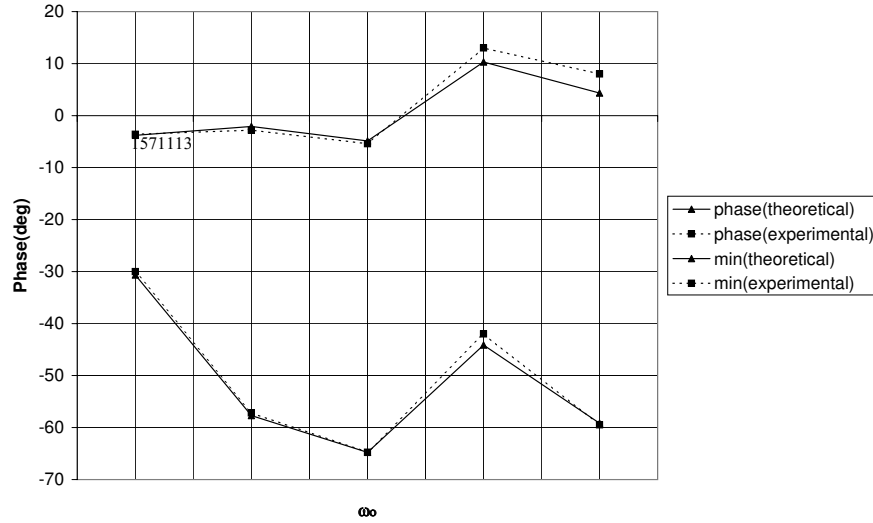


Figure 4.10: Comparison of the proposed repetitive scheme phase shift with LPF modification (bottom plot) before and (top plot) after  $\Delta\tau_d$ -compensation for  $K_1 = 0.88$  and  $K_2 = 0.9$ .

Figure 4.10 presents comparison of experimental and theoretical results of the proposed repetitive scheme before and after the  $\Delta\tau_d$ -compensation. In the top plot (dashed line) the phase shift after the  $\Delta\tau_d$ -compensation obtained experimentally is presented. In the top plot (solid line) the phase shift after the  $\Delta\tau_d$ -compensation obtained theoretically is shown. In the bottom plot (dashed line) the phase shift before  $\Delta\tau_d$  compensation obtained experimentally is presented as well as the phase shift before  $\Delta\tau_d$  compensation obtained theoretically (solid line). It is observed that theoretical values are very close to the experimental values. A considerable reduction of phase shift at  $6\ell \pm 1$  ( $\ell = 0, 1, 2, \dots, \infty$ ) harmonics after the  $\Delta\tau_d$ -compensation can be also observed from this comparison.

## 5. CONCLUDING REMARKS

In this thesis work a repetitive scheme intended for compensation of harmonics  $6\ell \pm 1$  ( $\ell = 0, 1, 2, \dots, \infty$ ) of the fundamental frequency  $\omega_0$  was presented. The idea behind the derivation of this scheme consisted in the nesting of a positive feedback repetitive scheme to a synchronous frame rotating at frequency  $\omega_0$ .

The positive feedback scheme (also well known as hyperbolic cotangent) was designed to produce an infinite set of resonance peaks tuned at frequencies  $6\ell\omega_0$ , which after the frequency shifting associated with rotations in a synchronous frame, produced resonance peaks of infinite gains at frequencies  $(6\ell \pm 1)\omega_0$  ( $\ell = 0, 1, 2, \dots, \infty$ ).

A considerable reduced expression was also obtained for the proposed repetitive scheme by applying the shifting frequency properties. The proposed repetitive scheme involved two delay lines (owning the same delay time), which were arranged in two feedback loops plus a feedforward path.

It was shown that after adding a damping gain to the proposed repetitive scheme a finite gain at the resonant peaks was obtained. As a consequence of this modification a slight phase shift appeared. To eliminate the phase shift at the resonant peaks, it was proposed to use two different damping gains, one for each delay line, namely,  $K_1$  and  $K_2$ , and a mathematical relation between  $K_1$  and  $K_2$  was found to guarantee a zero phase shift.

It was also shown that the proposed repetitive scheme was passive and that after the damping gain modification it became strictly passive.

Introduction of a LPF to the repetitive scheme was recommended to get rid of frequency sample noise during the digital implementation. This modification caused an important phase shift at resonant peaks. To overcome this issue a compensation strategy was proposed. It consisted in the introduction of an increment  $\epsilon$  in the delay

time of each delay line.

Experimental results were shown that proved the capabilities of the proposed repetitive scheme as well as its performance after damping gain and LPF modification.

### 5.1 Future work

In this thesis work the passivity properties of the proposed repetitive scheme were presented. These passivity properties were obtained for the regular  $(6\ell \pm 1)\omega_0$  ( $\ell = 0, 1, 2, \dots, \infty$ ) scheme and the  $(6\ell \pm 1)\omega_0$  ( $\ell = 0, 1, 2, \dots, \infty$ ) scheme after damping gain modification (introduction of gain  $K$ ). For future work, study of the repetitive scheme passivity properties after damping gain modification involving  $K_1$  and  $K_2$  is proposed.

The study of the repetitive scheme passivity properties after LPF modification is also left for future investigation. In this work it was observed that the Nyquist plot of the proposed repetitive scheme was on the right hand side of the complex plane, nevertheless a formal proof is needed to settle down the modified scheme passivity properties.

## 6. APPENDIX A

According to Figure 2.2 output  $Y$  is given by

$$\begin{aligned}
 y &= \rho_\ell^T \int_0^t \begin{bmatrix} h(\tau) & 0 \\ 0 & h(\tau) \end{bmatrix} \rho_\ell u(t - \tau) d\tau \\
 &= \int_0^t \rho_\ell^T \begin{bmatrix} h(\tau) & 0 \\ 0 & h(\tau) \end{bmatrix} \rho_\ell (t - \tau) u(t - \tau) d\tau \\
 &= \int_0^t h(\tau) \cos(\omega_0 \tau) u(t - \tau) d\tau
 \end{aligned}$$

Notice that, this convolution function describes systems with impulse response given by

$$\sigma(t) = h(\tau) \cos(\ell\omega_0 t) \tag{6.1}$$

and input  $u$ . In what follows the following frequency shifting property of the Laplace transform is used.

$$\mathcal{L}(h(\tau) \cos(\ell\omega_0 t)) = \frac{1}{2}H(s - \ell\omega_0 t) + \frac{1}{2}H(s + \ell\omega_0 t) \tag{6.2}$$

Where  $H(s) = \mathcal{L}\{h(t)\}$  and  $j = \sqrt{-1}$ . Therefore in the frequency domain, that is, applying the Laplace transform, using the preceding property, the following result is obtained

$$Y(s) = \Sigma(p)U$$

where  $\Sigma(s) = \frac{1}{2}H(s - \ell\omega_0 t) + \frac{1}{2}H(s + \ell\omega_0 t)$  and  $U = \mathcal{L}\{u\}$ .



## 7. APPENDIX B

According to Figure 2.3, the positive sequence component of the output  $Y_{\alpha\beta}$  is given by

$$\begin{aligned}
 y_{\alpha\beta}^p &= e^{Jl\omega_0 t} \int_0^t \begin{bmatrix} h(\tau) & 0 \\ 0 & h(\tau) \end{bmatrix} e^{-Jl\omega_0 \tau} u_{\alpha\beta}(t - \tau) d\tau \\
 &= \int_0^t e^{Jl\omega_0 t} \begin{bmatrix} h(\tau) & 0 \\ 0 & h(\tau) \end{bmatrix} e^{-Jl\omega_0 \tau} u_{\alpha\beta}(t - \tau) d\tau \\
 &= \int_0^t \begin{bmatrix} h(\tau) & 0 \\ 0 & h(\tau) \end{bmatrix} e^{Jl\omega_0(t-\tau)} u_{\alpha\beta}(t - \tau) d\tau \\
 &= \int_0^t \begin{bmatrix} h(\tau) \cos(\omega_0 \tau) & -h(\tau) \sin(\omega_0 \tau) \\ h(\tau) \sin(\omega_0 \tau) & h(\tau) \cos(\omega_0 \tau) \end{bmatrix} u_{\alpha\beta}(t - \tau) d\tau \\
 e^{Jl\omega_0 t} &= \begin{bmatrix} \cos(l\omega_0 t) & -\sin(l\omega_0 t) \\ \sin(l\omega_0 t) & \cos(l\omega_0 t) \end{bmatrix} \tag{7.1}
 \end{aligned}$$

while the negative sequence component of the output  $Y_{\alpha\beta}^n$  is given by

$$\begin{aligned}
 y_{\alpha\beta}^n &= \int_0^t \begin{bmatrix} h(\tau) & 0 \\ 0 & h(\tau) \end{bmatrix} e^{-Jl\omega_0 \tau} u_{\alpha\beta}(t - \tau) d\tau \\
 &= \int_0^t \begin{bmatrix} h(\tau) \cos(\omega_0 \tau) & h(\tau) \sin(\omega_0 \tau) \\ -h(\tau) \sin(\omega_0 \tau) & h(\tau) \cos(\omega_0 \tau) \end{bmatrix} u_{\alpha\beta}(t - \tau) d\tau
 \end{aligned}$$

The total output  $Y_{\alpha\beta}$  is composed of the sum of both sequence components, that



is

$$\begin{aligned} Y_{\alpha\beta} &= y_{\alpha\beta}^n + y_{\alpha\beta}^p \\ &= \int_0^t \begin{bmatrix} 2h(\tau) \cos(\omega_0\tau) & 0 \\ 0 & 2h(\tau) \cos(\omega_0\tau) \end{bmatrix} u_{\alpha\beta}(t - \tau) d\tau \end{aligned}$$

Therefore, each coordinate of the output,  $y_\alpha$  and  $y_\beta$ , is described by

$$\begin{aligned} y_\alpha &= 2 \int_0^t h(\tau) \cos(\omega_0\tau) u_\alpha(t - \tau) d\tau \\ y_\beta &= 2 \int_0^t h(\tau) \cos(\omega_0\tau) u_\beta(t - \tau) d\tau \end{aligned}$$

Notice that, this convolution function describes systems with impulse response given by

$$\sigma(t) = h(\tau) \cos(\ell\omega_0 t) \quad (7.2)$$

and input  $u_\alpha$  and  $u_\beta$ , respectively. In what follows the following frequency shifting property of the Laplace transform is used.

$$\mathcal{L}\{h(\tau) \cos(\ell\omega_0 t)\} = \frac{1}{2}H(s - \ell\omega_0 t) + \frac{1}{2}H(s + \ell\omega_0 t) \quad (7.3)$$

Where  $H(s) = \mathcal{L}(h(t))$  and  $j = \sqrt{-1}$ . Therefore in the frequency domain, that is, applying the Laplace transform, using the preceding property, the following result is obtained

$$Y_{\alpha\beta}(s) = \begin{bmatrix} 2\Sigma(s) & 0 \\ 0 & 2\Sigma(s) \end{bmatrix} U_{\alpha\beta}(s)$$

where  $\Sigma(s) = \mathcal{L}\{\sigma(t)\}$  and  $U = \mathcal{L}\{u_{\alpha\beta}\}$ .

## 8. THESIS CONTRIBUTIONS

The following documents are the contributions arisen from this thesis work.

- P.G. Hernández-Briones, G. Escobar, R. Ortega, M. Hernández-Gómez, “On the passivity properties of a new family of repetitive (hyperbolic) controllers,” *International Journal of Control*, in process.
- G. Escobar, P.G. Hernández-Briones, R.E. Torres-Olguín, A.A. Valdez, M. Hernández-Gómez, “A repetitive-based controller for the compensation of  $6\ell \pm 1$  harmonic components,” *ISIE 2007*, June 1007, Vigo, Spain.
- G. Escobar, P.G. Hernández-Briones, M. Hernández-Gómez, “Repetitive controller to compensate for  $6\ell \pm 1$  harmonics,” *US patent docket No. 1009.001*, USA, in process.



## BIBLIOGRAPHY

- [1] G. Escobar, P.R. Martínez and J. Leyva-Ramos , “Analog Circuits to Implement Repetitive Controllers with Feedforward for Harmonic Compensation,” *IEEE Trans. on Industrial Electronics*, Vol. 54(1), pp. 567-573, February 2007.
- [2] S. Hara, T. Omata and M. Nakano. “Synthesis of repetitive control of a proton synchrotron magnet power supply,” in *Proc. 8th World Congr. IFAC*, 1981, Vol. XX, pp. 1387-221.
- [3] S. Hara, T. Omata and M. Nakano. “Synthesis of repetitive control systems and its applications,” in *Proc. 24th Conf. Decision and Control*, 1985, Vol. 3, pp. 1387-1392.
- [4] B. Francis and W. Wonham. “The internal model principle for linear multivariable regulators,” *Applied Mathematics and Optimization*, Vol. 2, pp. 170-194, 1975.
- [5] Kequin Gu, Vladimir L. Kharitonov, Jie Chen, “Stability of Time-Delay Systems,” 1st edition, Birkhäuser Boston, 2003.
- [6] T. Inoue, M. Nakano, T. Kubo, S. Matsumoto, and H Baba. “High accuracy control of a proton synchrotron magnet power supply”. *Proceedings of IFAC world congress*, 1981, pp. 216-220.
- [7] S. Hara, Y. Yamamoto, T. Omata and M. Nakano. “Repetitive control systems: A new type servo systems and its applications,” *IEEE Trans. Automat. Contr.*, Vol. 33(7), pp. 659-667, 1988.
- [8] M. Tomizuka, T. Tsao and K. Chew. “Discrete-time domain analysis and synthesis of repetitive controllers,” In *Proc. American Control Conf.*, 1988, pp. 860-866.
- [9] R. Costa-Castelló and R. Griño, “A Repetitive Controller for Discrete-Time Passive Systems,” *Automatica*, Vol. 42, pp. 1605-1610, 2006.

- [10] G. Escobar, P.R. Martínez, J. Leyva-Ramos, and P. Mattavelli, "A negative feedback repetitive control scheme for harmonic compensation," *IEEE Trans. on Industrial Electronics*, Vol. 53(4), pp. 1383-1386, Jun 2006.
- [11] J. Leyva-Ramos, G. Escobar, P.R. Martinez and P. Mattavelli, "Analog Circuits to Implement Repetitive Controllers for Tracking and Disturbance Rejection of Periodic Signals," *IEEE Transactions on Circuits and Systems II: Express Briefs*, Vol. 52(8), pp. 466-470, August 2005.
- [12] D. Rice, "A Detailed Analysis of Six-Pulse Converter Harmonic Current". *IEEE Trans. on Industrial Electronics*, Vol. 30, pp. 294-304, 1994.
- [13] C.D. Schauder and S.A. Moran, "Multiple reference frame controller for active filters and power line conditioners," US Patent No. 5,309,353, USA, May 3, 1994.
- [14] Ogata, K., "Modern Control Engineering," 4th Edition, Prentice-Hall, 2002.
- [15] P. Mattavelli, "Synchronous-frame harmonic control for high-performance AC power supplies," *IEEE Trans. on Industry Applications*, Vol. 37(3), pp. 864-872, May/June 2001.
- [16] T.W. Rowan and R.J. Kerkman, "A new synchronous current regulator and an analysis of current-regulated PWM inverters," *IEEE Trans. on Industry Applications*, Vol. IA(22), pp. 678-690, July/Aug. 1986.
- [17] C.D. Schauder and R. Caddy, "Current control of voltage source inverters for fast four quadrant drive performance," *IEEE Trans. on Industry Applications*, Vol. IA(18), pp. 163-171, May/Apr. 1982.
- [18] M. Bojrup, P. Karlsson, M. Alakula and L. Gertmar, "A multiple rotating integrator controller for active filters," in *Proc. European Power Electronics Conf. EPE*, 1999, pp. 1-9, Lausanne, Switzerland.
- [19] I. Etxeberria-Otadui, A. Lopez-de-Heredia, H. Gaztañaga, S. Bacha and R. Reyer, "A single synchronous frame hybrid (SSFH) multifrequency controller for power active filters," *IEEE Trans. on Industrial Electronics*, Vol. 53(5), pp.1640-1648, Oct 2006.

- 
- [20] D.N. Zmood, D.G. Holmes and G. Bode, "Frequency domain analysis of three phase linear current regulators," in *Conf. Rec. IEEE-IAS Annual Meeting*, Phoenix, AZ, Oct 1999, pp. 818-825.
- [21] C.B. Jacobina, R.O. de Carvalho Jr., M.B.R. Correa, A.M.N. Lima and E.R.C da Silva, "Digital current controller of unbalanced three-phase power electronic systems," in *Proc. IEEE Power Electronics Specialists Conference PESC*, Galway, Ireland, 2000, Vol. 2, pp. 767-772, .
- [22] S. Fukuda and T. Yoda, "Investigation of current controller for single phase PWM converters based on the internal model principle," in *Proc. European Power Electronics Conf. EPE*, Lausanne, Switzerland, 1999, pp. 1-8.
- [23] S.Fukuda and T.Yoda. "A Novel Current Tracking Method for Active Filters Based on a Sinusoidal Internal Model", 35<sup>th</sup> *IAS Annual Meeting*, Rome, Oct 2000.
- [24] X. Yuan, W. Merk, H. Stemmler and J. Allmeling, "Stationary-frame generalized integrators for current control of active power filters with zero steady-state error for current harmonics of concern under unbalanced and distorted operating conditions," *IEEE Trans. on Industry Applications*, Vol. 38(2), pp. 523-532, March/April 2002.
- [25] G. Escobar, A. Stankovic and P. Mattavelli, "An Adaptive Controller in Stationary Reference Frame for D-Statcom in Unbalanced Operation" *IEEE Transactions on Industrial Electronics*, Vol. 51(2), pp. 401-409, April 2004.
- [26] G. Escobar, A.M. Stankovic and P. Mattavelli, "Adaptive controller for D-statcom in the stationary reference frame to compensate for reactive and harmonic distortion under unbalanced conditions," US Patent No. 6,862,199 B2, USA, March 1, 2005.
- [27] Bayard, David S, "A general theory of linear time invariant adaptive feedforward systems with harmonic regressors," *IEEE Transactions on Industrial Electronics*, Vol. 18(4), pp. 1056-1062, Jul 2003.
- [28] I. S. Gradshteyn and I.M. Ryzhik. *Table of integrals, series, and products*, 6th Ed., Academic Press, USA, 2000.

- [29] C. Xiao, D. J. Hill, "Generalization and new proof of the discrete-time positive real lemma and bounded real lemma," *IEEE Trans. on Circuits and Systems I*, Vol 46, No. 6, pp. 740-743, Jun 1999.
- [30] A. de Rinaldis, R. Ortega, M. Spong. "A Compensator for Attenuation of Wave Reflections in Long Cable Actuator-Plant Interconnections with Guaranteed Stability", March 2006.
- [31] J. H. Taylor, "Strictly positive-real functions and the Lefschetz-Kalman-Yakubovich (LKY) lemma," *IEEE Trans. on Circuits and Systems*, pp. 310-311, March 1974.
- [32] P. Ioannou, G. Tao, "Frequency domain conditions for strictly positive real functions", *Trans. on Automatic Control*, Vol AC-32, No. 1, pp. 53-54, January 1987.